Final Report

Analysis of Satellite Measurements to Improve California's Models for O_3 and PM

CARB 06-328

Principal Investigator

Ronald C. Cohen

Professor, Department of Chemistry and
Department of Earth and Planetary Science
University of California, Berkeley
Berkeley, CA 94720-1460
(510) 642-2735
(510) 643-2156 (FAX)
e-mail: rccohen@berkeley.edu

Report prepared for:

State of California Air Resources Board
Research Division
PO Box 2815
Sacramento, CA 95812

October 2010

Acknowledgements

The measurements described in this report were obtained using the OMI instrument (manufactured by the Dutch Space Agency) aboard the NASA AURA satellite. We have made use of column NO_2 from the NASA standard product and the KNMI DOMINO product in our analyses. Both products are available freely on the web. We thank our colleagues at KNMI and NASA for their cooperation and helpful discussions during the course of this work. Part of the work in the report was performed by Luke Valin funded in part by the NASA Earth and Space Science Fellowship Program.

Disclaimer

The statements and conclusions in this report are those of the authors from the University of California and not necessarily those of the California Air Resources Board. The mention of commercial products, their source, or their use in connection with the material reported herein is not to be construed as actual or implied endorsement of such products.

Table of Contents

Abstract **7**

Executive Summary **8**

1. Introduction **10**

2. Satellite observations of NO_2 Columns **11**

3. Surface and aircraft measurements **13**

Surface network *13*

Aircraft Observations *14*

4. Emission inventories and WRF-CHEM **14**

Emissions Inventory *14*

WRF-CHEM *14*

5. Space-based Constraints on Spatial and Temporal Patterns of NOx Emissions in California, 2005-2008 **15**

Day-of-week patterns in NO_2 *16*

Year-to-year trends in NO_2 *19*

Estimates of Uncertainty in OMI Observations *21*

Space-based constraints on Emission Inventories *22*

Conclusions about CA emissions *23*

6. Effects of spatial resolution on model/satellite comparisons **25**

Illustration using a 1-D plume model *26*

Illustration using a 2-D plume model *28*

NO_2 biases calculated with WRF-CHEM *30*

Summary of effects of model resolution on comparison of satellite and model NO_2 columns *32*

7. Emerging uses of Satellite NO_2 columns **33**

Spatial patterns in the "weekend" effect and model chemistry *33*

Effects of meteorology on model/satellite NO_2 comparisons *34*

Variation of column NO_2 from 1 to 1:30 PM *36*

Comparison of OMI columns to aircraft observations during ARCTAS-CARB *38*

Refined retrieval *39*

8. Conclusions and Recommendations **40**

9. References **42**

10. Glossary of Terms, Abbreviations, and Symbols **47**

List of Figures

Figure 1:	Satellite observations of column NO_2: from observations of single overpasses to seasonal averages	11
Figure 2:	Average summertime NO_2 column for weekdays in 2005, weekends in 2005, and weekdays in 2008.	15
Figure 3:	Average summertime weekday/weekend ratio for 2005-2008 observed by OMI	16
Figure 4:	Average weekly profiles of NO_2 for summer months (June-August) from OMI and from CARB monitoring sites	17
Figure 5:	Average tropospheric weekday and weekend NO_2 column observed by OMI and CARB from 2005-2008 over select air basins.	19
Figure 6:	Percent change in emissions from CARB inventory versus change in OMI tropospheric NO_2 for 2005-2008 and select air basins.	21
Figure 7:	Source distribution of emissions for weekdays and weekends over select air basins.	25
Figure 8:	Analytical model of OH and NO_2 lifetime versus NO_2	26
Figure 9:	1-D plume model of column NO_2 and corresponding OH feedback	27
Figure 10:	Resolution-dependent biases of NO_2 simulated in 1-D	28
Figure 11:	2-D plume model of a conserved tracer and NO_2	29
Figure 12:	Resolution-dependent bias of NO_2 from a point source simulated in 2-D at four spatial scales	30
Figure 13:	Column NO_2 simulated at 4 km over California with WRF-CHEM and biases of ±25% at 12, 96 and 192 km resolution.	31
Figure 14:	Column NO_2 simulated at 4 km over the Southwest US with WRF-CHEM and biases of ±25% at 12, 96 and 192 km resolution.	32
Figure 15:	Percent biases in WRF-CHEM predicted NO_2 column	32
Figure 16:	Attempts to simulate the OMI-observed spatial pattern in the ratio of weekday:weekend column NO_2 using WRF-CHEM over California	34
Figure 17:	Variation of OMI-observed column NO_2 versus wind over Four Corners and San Juan Power plants	35
Figure 18:	Variation of OMI-observed column NO_2 versus wind over San Francisco Bay Area	36
Figure 19:	Change in column NO_2 from 1 to 1:30 PM observed by OMI and simulated by WRF-CHEM over the Los Angeles Basin	37
Figure 20:	Comparison of NO_2 vertical column densities obtained from boundary layer aircraft observations to satellite observations	38
Figure 21:	Comparison of NO_2 aircraft and satellite vertical column densities for the standard product and revised retrievals	40

List of Tables

Table 1: Daily concentrations relative to average weekday concentrations of NO_2 for summers 2005-2008 for OMI and the CARB inventory, and for summers 2005-2007 for the CARB surface observations 18

Table 2: Average percent change NO_2 per year for each season from 2005-2008. 23

Table 3: Terrain reflectivity, pressure and NO_2 vertical profile inputs for satellite column NO_2 retrievals. 39

Abstract

Satellite based UV-visible spectroscopy measuring NO_2 is now routine and prospects for continuing observations are excellent. We performed an extensive analysis of the application of satellite measurements to an understanding of spatial and temporal patterns of NO_2 in California. The analysis confirms that trends observed from space are extremely accurate—inter-annual variations as small as 1-2% are evident in a time series. We find that interpretation of the satellite record requires attention to both the spatial resolution of the primary observations and the model used to interpret those observations. We note that the spatial pattern of the satellite observations from the OMI instrument varies in a 16 day sequence, so that long term averages can be constructed that have higher resolution than the original observations. This spatial pattern is sensitive to emissions, meteorology and chemistry and is one of the most informative tests we have available of the accuracy of the components of current air quality models. We describe application and evaluation of the satellite observations with attention to trends in major air districts in California and with an eye to new strategies for integrating satellite observations into the air quality management system.

Executive Summary

We describe a series of analyses of space based measurements of NO_2 columns over California. The evidence is compelling that the observations are an accurate reflection of trends in NO_2 by day-of-week and from year to year, and that seasonal and monthly averages of the measurements provide exquisitely detailed spatial maps and provide insight into the differences in emissions in different regions of the state. Individual column measurements are accurate to roughly 50%. While not yet sufficiently accurate to be used for regulatory purposes, the trends (comparing a time series in the same month/season over many years or comparing days of week in a single location) and the spatial patterns observed are quite accurate, making them better than any other data set we are aware for evaluation of models and emissions inventories, and for assessing the progress of existing regulatory initiatives. The satellite observations also provide unambiguous measurements of the location of plume edges. Locating the edges is not possible with the surface network.

In this report, we describe the Ozone Monitoring Instrument (OMI) and make brief mention of other instruments. We describe an extensive comparison to the CARB surface network and a preliminary comparison to aircraft observations both of which support the conclusion that the OMI measurements accurately capture trends in space and time. We provide an extended analysis (adapted from Russell et al. 2010), of ground and space-based measurements of spatial and temporal variation of NO_2 in four California metropolitan regions. The measurements of weekly cycles and trends over the years 2005-2008 observed both from the surface and from space are nearly identical to each other, with small differences that can be accounted for by OH feedback on NO_2. As NO_x emissions are decreased in these urban, high NO_x regimes, OH concentrations increase, decreasing the lifetime of NO_2 and thereby compounding the observed decrease in NO_2 column. Satellite-observed decreases in Los Angeles and the surrounding cities are 46% on weekends and 9% per year from 2005-2008. Similar decreases are observed in the San Francisco Bay area and in Sacramento. In the San Joaquin Valley cities of Fresno and Bakersfield weekend decreases are much smaller, only 27%, and the decreasing trend is only 4% per year. We describe evidence that the satellite observations provide a uniquely complete view of changes in spatial patterns over time. For example, we observe variations in the spatial pattern of weekday-weekend concentrations within the Los Angeles basin with much steeper weekend decreases at the eastern edge of the basin than at the coast. We also observe that the spatial extent of high NO_2 in the San Joaquin Valley has not receded as much as it has for other regions in the state. Analysis of these measurements is used to describe observational constraints on temporal trends in emission sources in the different regions.

Interpretation of satellite columns remains a subject that requires more research. We describe the effects of spatial resolution on model predictions of NO_2 column and thus on the inference of emissions based on those comparisons, concluding that resolution of 24 km is too coarse, 12 km is too coarse for certain source types, but that 4 km is adequate for comparison to the satellite observations over all sources with the possible exception of the largest point sources. We then describe a series of research topics that were explored during this contract.

- We find that reproducing time-of-day and day-of-week variations in satellite column NO_2 with WRF-CHEM is an especially stringent test of model performance and that both NO_x and VOC emissions affect these variations. We recommend further research aimed at using both day-of-week and seasonal variations in NO_2 column as constraints on model performance.
- We describe the effects of meteorology, specifically wind speed, on the retrieved NO_2 column.
- We show that OMI observes changes in column NO_2 from 1:00-1:30 PM. We compared the measured change to changes predicted by WRF-CHEM.

- We describe elements of a strategy aimed at an improved retrieval of NO_2 column from the measured spectrum and we describe comparison of the NO_2 column using a standard analysis and improved retrievals to observations made during the ARCTAS-CARB experiments.

Analysis of Satellite Measurements to Improve California's Models for O_3 and PM

1. Introduction

Nitrogen oxide (NO_x = NO + NO_2) emissions contribute to production of O_3, inorganic and organic aerosol, and to violation of health-based ozone and aerosol standards in many communities. In some locations NO_2 itself exceeds health-based standards. In California, efforts to reduce O_3 and aerosol by reducing their chemical precursors (NO_x, volatile organics and directly emitted particles) have resulted in significant improvements in air quality (Board, 2009). However, concentrations of ozone and aerosol still remain higher than the regulatory limits over the most populous parts of the state. Current predictions suggest that new regulations will yield further decreases in these emissions and in O_3 and aerosol.

Confirming that control strategies are reducing emissions as predicted remains difficult, however, because observing networks are sparse. Concentrations at any particular location are affected by multiple changes in human activity, including emission reductions, population changes, changes in miles driven, etc. Gaps in the density of surface networks make conclusions about the spatial extent of emission reductions subject to debate because changes in the spatial distribution of emissions over time are not uniformly recorded. Observations of nitrogen oxides from space offer a new perspective, one with complete spatial coverage that is not subject to the limitations of the sparse surface network.

This contract was aimed at evaluating the potential for using observations from the Ozone Monitoring Instrument (OMI), which achieves daily global coverage and has high spatial resolution (13 km × 24 km at nadir; 24 × 128 at the edge of the sampling swath), to study spatial and temporal variability in NO_2 concentrations in California. We evaluate the capacity of using satellite observations to act as a check on models and emissions inventories and for assessing the progress achieved by current regulatory efforts.

We completed the following objectives with support from this contract and also with contributions from a NASA ESSF to Luke Valin. This work also builds on parallel research aimed at other cities/locations performed for NASA during the time when this contract was suspended:

1) We completed development of code that produces an area weighted average of individual observations resulting in high resolution (~7 x 7 km) images at seasonal resolution (separately for weekdays and weekends).
2) We investigated whether the instrument is sensitive to variations in NO_2 column at different times of day.
3) We investigated the spatial resolution of the sensor including a) the resolution of the area weighted image, b) the effects of model resolution on OH chemical feedback to NO_2 column and c) the effects of resolution of a priori assumptions on column retrieved from the OMI spectrum. In parallel, we investigated the effects of model resolution on predictions of column NO_2 for both point and area sources.
4) We investigated the effects of meteorology on NO_2 columns using observations.
5) We used WRF-CHEM predictions of column NO_2 to provide insight into the factors affecting variation in the column and to guide our understanding of which elements of a model can be constrained by the column NO_2 observations.

6) We developed a comparison of surface network and satellite trends, and a comparison of satellite column to aircraft observations from ARCTAS-CA.

These analyses and the tools used to develop them are described in the following report.

2. Satellite observations of NO_2 Columns

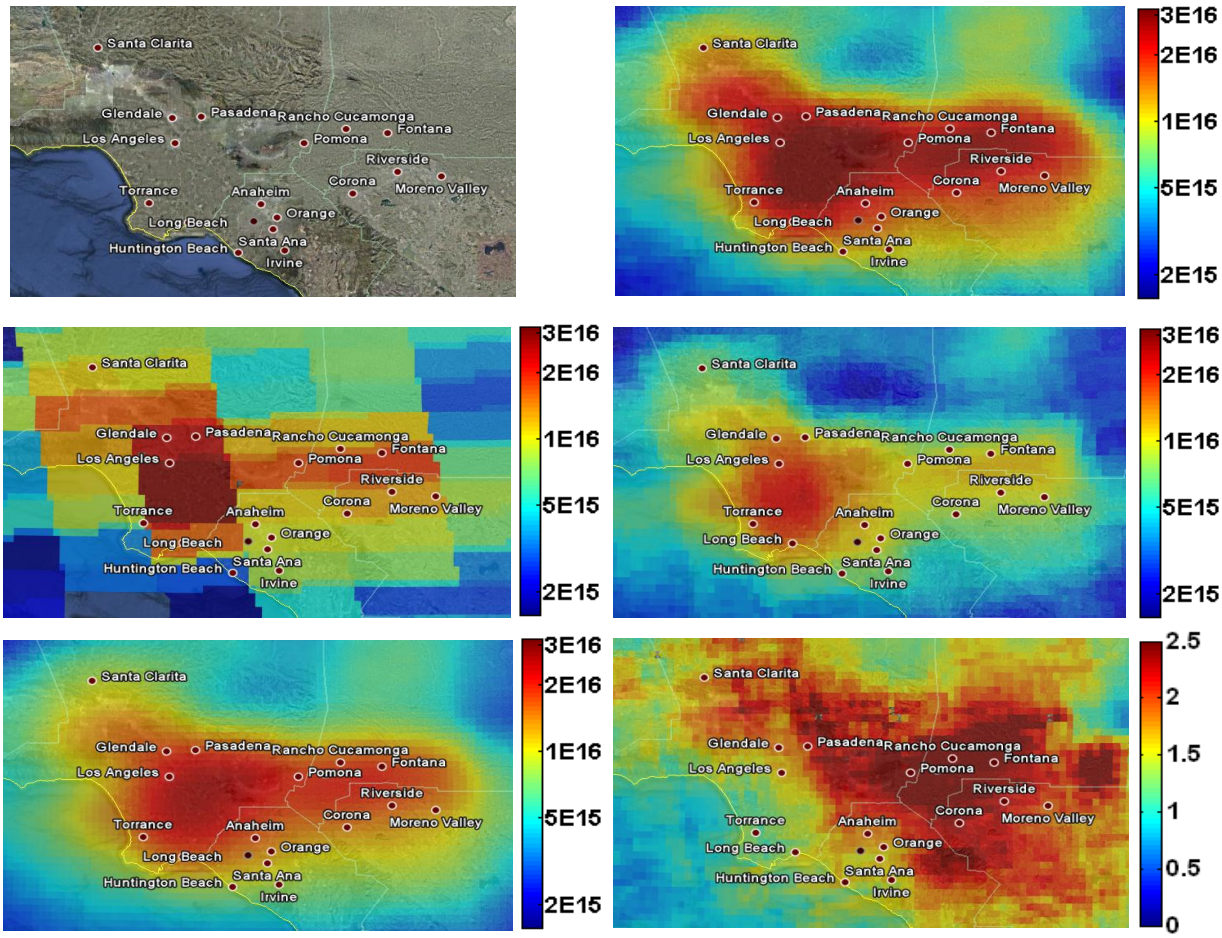

Figure 1. (top left) Google earth image of South Coast Region of California. (center-left) Tropospheric column NO_2 concentrations (molecules cm^{-2}) from the Ozone Monitoring Instrument (OMI) over the South Coast region of California from one day, August 1, 2008. Overlap of coverage in the flight direction (North-South) produces thin stripes which arise from averaging of subsequent pixels. OMI tropospheric NO_2 columns (molecules cm^{-2}) averaged over summer months (Jun-Aug) for the years 2005-2008 at 0.025 degree resolution for (bottom left) weekdays and weekends, (top right) weekdays only, (center right) weekends only, and (bottom right) ratio of weekday to weekend.

The Ozone Monitoring Instrument (OMI) is a UV/Vis spectrometer orbiting sun-synchronously aboard the AURA satellite. The Aura satellite travels roughly 705 km above the surface of the Earth in a sun synchronous, polar orbit. It passes over North America at roughly 13:45 local time. The 114 degree viewing angle of the telescope yields a 2600 km swath on the ground, allowing the instrument to achieve near-global coverage each day in roughly 15 orbits (Levelt et al., 2006) . The detector is an 814 × 578 charge-coupled device (CCD) array that simultaneously records the spectral information in one dimension and spatial information in the second (Dobber et al., 2005; Levelt et al., 2006). Five individual 0.4-s exposures are integrated to achieve a 13 km spatial resolution in the flight direction at nadir. The spatial dimension is averaged on board to 60 pixels. Pixel sizes perpendicular to the flight direction vary from 24 km at nadir to 128 km

at the edges of the swath. Analyses of the spectra provide observations of the column abundances of NO_2, O_3, CH_2O, CHOCHO, and cloud and aerosol properties.

In most of our work, we use column NO_2 data archived by NASA. The tropospheric NO_2 column from this source is known as the "Standard Product" (Level 2, Version 1.0.5, Collection 3) and it is available from the NASA Goddard Earth Sciences (GES) Data and Information Services Center (DISC) (http://disc.sci.gsfc.nasa.gov/Aura/data-holdings/OMI/omno2_v003.shtml). In some analyses we compare to a different publicly available retrieval known as the Near-Real-Time product provided by the Netherlands Royal Meteorological Institute (KNMI) described in Boersma et al. (2007). The Near-Real-Time product makes different assumptions about how to produce an optimal retrieval**.** These variations lead to differences that have been significant for other analyses (Bucsela et al., 2008; Hains et al., 2010; Lamsal et al., 2010). We report results from the Standard Product here, highlighting differences from the KNMI product where relevant. We also developed our own retrieval algorithm as a means to investigate the assumptions used in the two publically available products.

The standard product retrieval uses a modified Differential Optical Absorption Spectroscopy (DOAS) procedure to determine slant column densities of NO_2 using a non-linear least squares fit on the ratio of measured earthshine radiance to solar irradiance spectrums in the 405-465 nm window. Details concerning the Standard Product retrieval of NO_2 vertical column densities from raw spectral measurements are provided in Boersma et al. (2002), Bucsela et al. (2006), and Celarier et al. (2008). Briefly, the slant column densities are converted into vertical column densities by applying an air mass factor (AMF); defined as the ratio of the slant column density to the vertical column density of NO_2. AMFs are determined as a function of viewing geometry, the reflectivity and pressure of terrain and clouds, and the NO_2 profile shape. Surface reflectivity is derived from GOME (Global Ozone Monitoring Experiment) observations and averaged monthly to 1° × 1° degree resolution (Koelemeijer et al., 2003). AMFs are calculated using both unpolluted (stratospheric and upper tropospheric) and "polluted" (lower tropospheric) NO_2 profiles. "Polluted" NO_2 profiles are determined from a geographically gridded set of annual mean profiles from a GEOS-Chem simulation at 2 × 2.5 degree resolution (Martin et al., 2003). Use of a single set of profiles in the standard product is an advantage because it ensures that trends in observations are not aliasing external information. However, the low resolution of the *a priori* information does introduce errors. An initial vertical column density is obtained using the unpolluted AMF. Unpolluted NO_2 column concentrations are then determined by masking areas of high tropospheric NO_2 and applying a zonal planetary wave smoothing. The stratospheric column is then subtracted and the remaining slant column is converted to a vertical column using the "polluted" AMF. The resulting "polluted" column represents NO_2 near the surface in regions where NO_2 is elevated above background levels. The effect of clouds is accounted for by calculating AMFs for both clear and cloudy conditions and using a radiance-weighted sum of the cloudy and clear AMFs. Cloud information is acquired from the OMI O_2-O_2 cloud algorithm (Acarreta et al., 2004). In order to minimize the influence of clouds on NO_2 columns, data chosen for analysis has been filtered to exclude pixels with a cloud fraction exceeding 0.2. Our analyses were repeated using a 0.1 cloud fraction threshold with no significant change in the results.

Significant errors and biases in the OMI polluted column are dominated by uncertainties in the AMF determination and to a lesser extent by errors in the slant column fitting and stratospheric subtraction (Martin et al., 2002; Martin et al., 2003; Boersma et al., 2004). Wenig et al. (2008) estimates that the uncertainty in the standard product retrieval of tropospheric NO_2 is on the order of 40-80% for an individual observation. This is similar to 40% error due to AMF and absolute error of 1×10^{15} molecules cm^{-2} due to the stratospheric subtraction estimated by Martin

et al. (2006) for SCIAMACHY (SCanning Imaging Absorption spectroMeter for Atmospheric CHartographY) observations and the 35-60% error estimated by Boersma et al. (2004) for observations from GOME. Direct comparison to aircraft profiles suggests the upper range of these estimates are too high and that the true accuracy is more in the range of 30-50%.

OMI achieves complete global coverage each day with a repeat cycle of 16 days, such that for a given location, the NO_2 column is gathered by a different pixel within the 60 across track positions each day. Consequently, data are collected both at a different spatial resolution and with pixel centers at different locations each day. We take advantage of the shifting pattern of the pixels on the ground to produce a high resolution monthly average product. We use an area-weighted averaging, binning to 0.025° × 0.025°. We include the center 20 pixels from each swath to limit the measurements to those with a pixel size less than 15 × 27 km^2, eliminating pixels at the outer edges of the swath that have dimensions as large as 24 × 128 km^2. Although we omit two-thirds of the data, the maps we produce have much higher spatial resolution than maps that include the larger pixel size measurements. In Figure 1 (center left) we show OMI NO_2 columns for one summer day, August 1, 2008, and in Figure 1 (bottom left), the area-weighted average summer (June-August) concentration over four years (2005-2008). A thin, averaged region between two adjacent pixels is visible at fine resolution as shown in Figure (center left). These regions appear because the width of the OMI pixels in the flight direction vary from 13 km at the center of the scan line to about 24 km at the edges of the swath, producing an overlap along the flight direction for pixels at the outer part of the swath. Capturing these overlapping regions further increases the statistics in the analysis. Analysis shows that the higher resolution image (Figure 1 bottom left) has approximately 10 km spatial resolution and spatial precision of about 3 km (Valin et al., in preparation). As a rough guide to interpreting this figure, for a well-mixed 1 km boundary layer, a column of 1×10^{16} molecules cm^{-2} NO_2 corresponds to 3.7 ppb NO_2 at the surface.

3. Surface and aircraft measurements

Surface network

The California Air Resources Board (CARB) manages an extensive ground based network of monitors, ninety-four of which were recording hourly NO_2 concentration from 2005-2008. Measurements of surface NO_2 at these sites are provided by chemiluminescence analyzers equipped with molybdenum converters (Fontijn et al., 1970). Laboratory and field studies have shown that conversion by a molybdenum converter is not specific to NO_2 (Dunlea et al., 2007; Winer et al., 1974; Steinbacher et al., 2007). Substantial interferences arise from conversion of higher NO_x oxidation products including HNO_3, alkyl and multifunctional nitrates, and peroxyacetylnitrates. The conversion of these species to NO yields an overestimation in measured NO_2 concentration.

In order to evaluate how interferences affect the NO_2 concentration observed at surface monitoring sites in California, we compare measured surface level NO_2 concentrations with NO_2 determined using a photochemical steady-state calculation based on NO and O_3 measurements made at the same sites. As expected, we find that NO_2 concentrations determined using the photochemical steady-state calculation are lower than the NO_2 measurements. For this data set we find a typical bias of about 20%. We find that the disagreement between observations of NO_2 and the steady-state calculation is similar on weekdays and weekends and that there is no significant trend in the bias over the 2005 to 2008 period.

Limiting ourselves to sites with detectable NO for photochemical steady-state calculation of NO_2 substantially reduces sampling statistics. Since our comparison of satellite observations and surface measurements is focused on trends and not on comparison of absolute mixing ratios, and the error induced by the molybdenum converter measurement should be roughly constant over time for individual monitoring stations, we report NO_2 concentrations measured directly by the commercial analyzers (with no correction applied) in the remainder of this report.

Aircraft Observations

During the ARCTAS campaign (Jacob et al., 2010), in situ observations throughout the troposphere were obtained using the UC-Berkeley Laser-Induced Fluorescence (TD-LIF) instrument aboard NASA's DC-8 aircraft. Details concerning the instrument are provided in Thornton et al. (2000). Briefly, a tunable dye laser is pumped at 7 kHz by a Q-switched, frequency doubled Nd^{3+}:YAG laser. The incoming gas is cooled by supersonic expansion (Cleary et al., 2002) and the dye laser is tuned to an isolated rovibronic feature of jet-cooled NO_2 at 585 nm. The frequency is held for 9 s at the peak of this feature and then for 3 s at an offline position in the continuum absorption. The ratio of peak to background fluorescence of the chosen feature is 10 to 1 at 1 atm and the difference between the two signals is directly proportional to the NO_2 mixing ratio. The laser light is focused in series through two multi-pass cells and the red-shifted fluorescence is detected using a red-sensitive photomultiplier tube. Fluorescence counts are collected at 4 Hz, scattered light at wavelengths less than 700nm is rejected by band-pass filters and time-gated detection is used to eliminate noise resulting from scattered laser light in the cell. We observe a dependence of NO_2 fluorescence on the external pressure. We calibrate the NO_2 LIF vs. altitude by direct measurement of NO_2 from a standard addition during a test-flight. Calibrations were performed at least once every two hours during a level flight leg using a 4.7 ppm NO_2 reference gas with a stated certainty of +/− 5%. The precision of the mixing ratio observations at 1Hz is estimated to be ±23 ppt at 1000 hPa and ±46 ppt at 200 hPa (S/N=2) (Bucsela et al., 2008).

4. Emission inventories and WRF-CHEM

Emissions Inventory

Estimated emissions are obtained from the California Air Resources Board website (http://arb.ca.gov) and are divided into stationary, off-road mobile, on-road mobile, natural, and area-wide categories. We consider basin-wide emissions from the San Francisco Bay Area, the San Joaquin Valley, and the South Coast air basins and county-wide emissions from Sacramento County. On-road vehicle activity and emission information is obtained using the CARB's EMissions FACtors model (EMFAC2007 V2.3 Nov 1, 2006) (available at: http://arb.ca.gov/msei/onroad/latest_version.htm). The Emissions Factors (EMFAC) model accounts for activity-related information by utilizing vehicle registration data from the California Department of Motor Vehicles as well as other vehicle information from regional transportation agencies. Emissions are broken down into ten different vehicle classes, and within each of those classes, into non-catalyst equipped, catalyst equipped, and diesel subcategories. Exhaust and evaporative emissions are estimated and incorporated into the emission factors, along with county-specific activity data, including vehicle population, vehicle miles traveled, number of vehicle starts, ambient temperature and soak and activity distribution information.

WRF-CHEM

We run WRF-CHEM v3.1, a state-of-the-art multi-scale regional chemical transport model (CTM) with chemical transport driven "on-line" such that aerosols and trace gases can provide

feedback onto physical processes (Grell et al., 2005). Emissions supplied for WRF-CHEM are made up by the National Emission Inventory (NEI) 2005 onroad and offroad transportation emissions for a typical July weekday and Continuous Emissions Monitoring (CEMS) averaged point source emissions for a typical August 2006 weekday. For more information, see ftp://aftp.fsl.noaa.gov/divisions/taq/emissions_data_2005/Weekday_emissions/readme.txt. There are a variety of chemical mechanisms available for WRF-CHEM and a coupled Kinetic PreProcessor (KPP) (Sandu and Sander, 2006), which provides greater flexibility in modifying chemical mechanisms. Currently, we run simulations with chemistry driven by the mechanism developed for the Regional Acid Deposition Model, version 2 (Stockwell et al., 1990). Several biogenic emission modules exist for WRF-CHEM. We use a landuse-based online module for calculation of biogenic emissions as in (Grell et al., 2005). The model is driven by the North American Regional Reanalysis (NARR – http://nomads.ncdc.noaa.gov/dods/NCEP_NARR_DAILY).

5. Space-based Constraints on Spatial and Temporal Patterns of NOx Emissions in California, 2005-2008

Note: the bulk of this section was presented in (Russell et al., 2010).

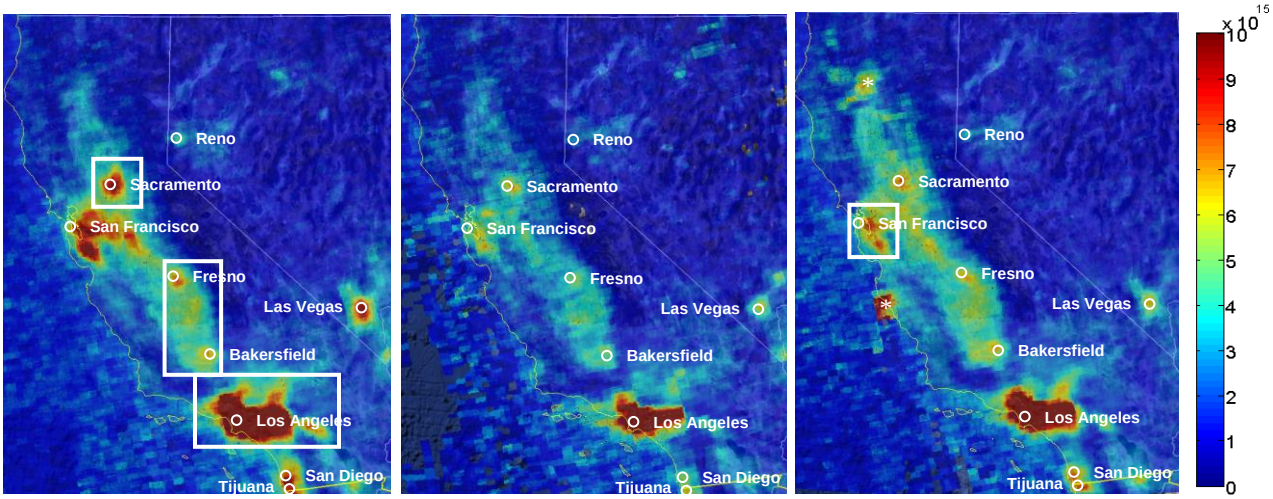

Figure 2. Average summertime OMI tropospheric NO_2 column concentrations (molecules cm^{-2}) for (left) a weekday (Tuesday-Friday) in 2005, (center) a weekend day (Saturday-Sunday) in 2005 and (right) a weekday in 2008.

To demonstrate and evaluate the OMI observations, we examine the observations over CA from 2005-2008 concentrating on four regions in California with the highest NO_x concentrations: Sacramento County, the San Francisco Bay Area air basin, the San Joaquin Valley air basin, and the South Coast air basin, shown as boxed regions in Figure 2. We focus primarily on summer months because the NO_x photochemical lifetime is shorter (~4 hr at noon). Consequently, we can expect both minimal carryover from the previous day and minimal transport from sources to regions downwind, yielding a column that is especially representative of local surface emissions. Further, the number of available satellite measurements is maximized during summer months when cloud cover is lowest. We define the area of analysis as that region where the NO_2 column in summer 2005 exceeded 6×10^{15} molecules cm^{-2} in the Sacramento, San Joaquin Valley, and South Coast regions. We use this threshold in order to specifically select urban regions where human activity makes a substantial impact on NO_2 concentrations while preventing the signal from being dampened by surrounding rural regions. In 2005, the San Francisco Bay Area urban plume extended east to blend with the plumes from other cities. To define the region of interest

for San Francisco, we use summer 2008 measurements where a separation between the basins is evident (see Figure 2 right panel). Based on inter-annual trends reported below, we adjust the threshold to 4.6×10^{15} molecules cm^{-2} for the 2008 measurements as we believe this is comparable to using the 6×10^{15} molecules cm^{-2} threshold for 2005 data. In the San Joaquin Valley, the threshold we use focuses attention on Fresno and Bakersfield. Separate analysis of these two cities leads to essentially identical conclusions.

Day-of-week patterns in NO_2

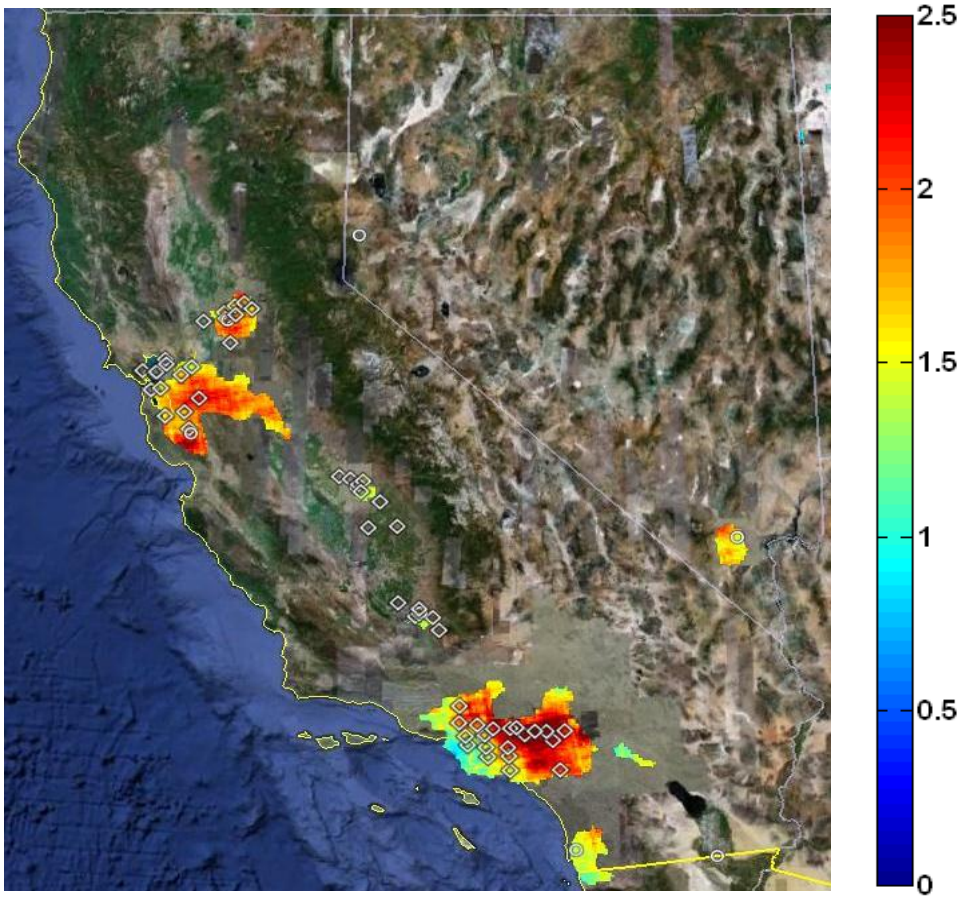

Figure 3. Average summertime weekday/weekend ratio for 2005-2008. Ratios for regions with weekday columns less than 6×10^{15} molecules cm^{-2} in summer 2005 are omitted. Locations of CARB surface NO_2 monitoring sites used in this study are marked with white diamonds.

Variation in the magnitude of NO_x emissions and NO_2 concentrations with day of week are well known and have been described using ground and spaced-based measurements (Cleveland et al., 1974; Gordon, 1994; Marr and Harley, 2002b, a; Harley et al., 2005; Murphy et al., 2007; Beirle et al., 2003; Kaynak et al., 2009; Kim et al., 2009). In the U.S. the effect is largely due to the decrease in heavy-duty diesel trucks on weekends, although changes in the timing of passenger vehicle traffic may contribute (Marr and Harley, 2002b; Murphy et al., 2007; Janssen and Carey, 1999). In Figure 2 (left and center) we show the difference in spatial patterns of the NO_2 column for weekdays and weekends across the State of California for the summer of 2005. We define weekdays as Tuesday-Friday, weekends as Saturday-Sunday, and summer as June-August. Observations indicate there is significant memory of the previous day's emissions, thus Saturday and Monday behave as intermediate between weekends and weekdays (see (Murphy et al., 2007)

for additional discussion of this effect). We omit Monday to reduce unnecessary bias in the weekday values but keep Saturday to enhance the statistics of our analysis of weekends. Retaining Saturdays has the effect of increasing the "weekend" values. On the other hand, cumulative emissions on Sunday prior to the satellite overpass time (roughly 1 PM) are only 40% of the daily total NO_x emissions while emissions are 55% prior to 1 PM for other days of the week (R. Harley, personal communication, October 23, 2009). These two factors are important to keep it in mind in the interpretation of the measurements.

Observations show elevated concentrations of NO_2 in and around highly populated areas, including the major California cities of Sacramento, San Francisco, Fresno, Bakersfield, Los Angeles, and San Diego and Reno and Las Vegas in Nevada and Tijuana in Mexico (Figure 2). In all of these regions, the NO_2 columns are higher on weekdays (Figure 2 left) than on weekends (Figure 2 center). Outside of these population hotspots, rural regions show no significant day-of-week variability in NO_2 column. Furthermore, we find relatively smaller weekend effects directly above regions with the highest columns and larger effects downwind. This feature is clearest in the South Coast basin as shown in more detail in Figure 1. OMI observes almost exactly the same columns over the ports of Los Angeles and Long Beach and over downtown Los Angeles on weekdays and weekends (weekday to weekend ratios of ~1.2) but sees a large weekend effect (weekday-weekend ratio of 2.5) east of Los Angeles. The ratio of weekday to weekend NO_2 columns exhibits much smaller variation in cities in the San Joaquin Valley (~1.3) than observed in the other urban regions of California or Nevada where ratios are typically greater than 1.5 (Figure 3)

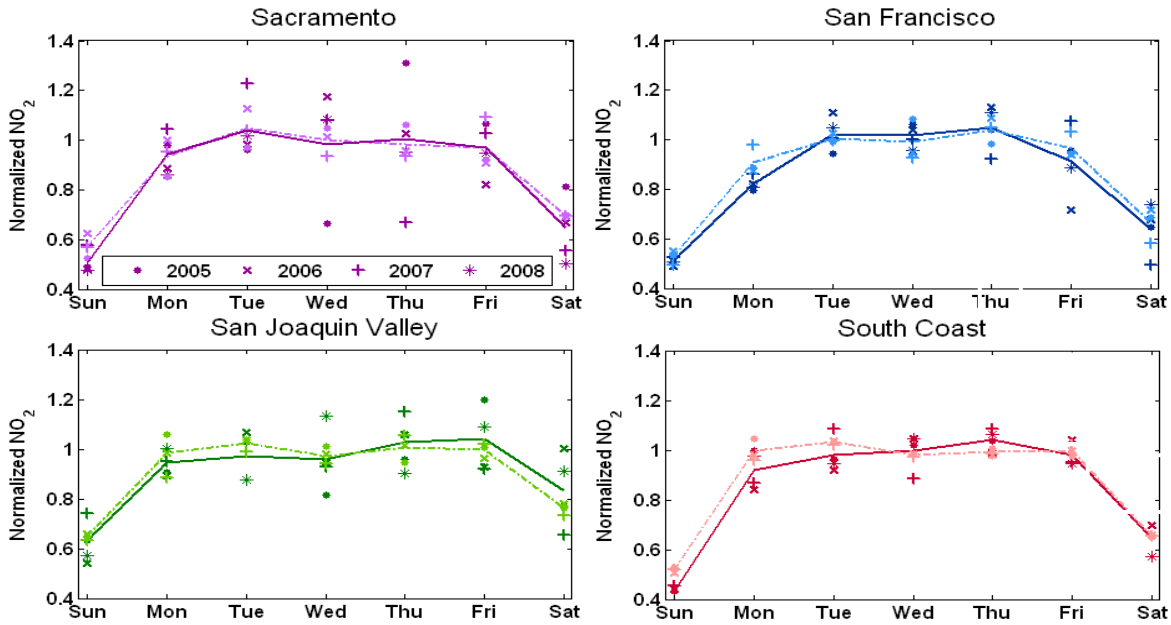

Figure 4. Average weekly profiles of NO_2 for summer months (June-August) from OMI (solid) and CARB monitoring sites (dashed) normalized to the average weekday (Tue-Fri) value. CARB data is for 2005-2007 while OMI data is for 2005-2008. Points show averages for individual years normalized to average weekday value for that year.

Figure 4 shows the summertime (Jun-Aug, 2005-2008) OMI NO_2 tropospheric columns and surface level NO_2 from the CARB air monitoring network (2005-2007) for each day of week, normalized to the weekday (Tuesday-Friday) average. We exclude major holidays (New Year's Eve & Day, Easter, July 4th, Veteran's Day, Thanksgiving and the day preceding, Christmas Eve & Day) from analysis as activity patterns tend to deviate from the average on these days. The CARB surface monitoring data for 2008 was not yet available at the time of analysis. Excluding

2008 OMI data does not affect our conclusions. Saturday values are lower than weekday values and a Sunday minimum is observed in all four regions and in both datasets. Differences in Saturday versus Sunday emissions and/or the effects of carry-over from the previous day are likely responsible (Murphy et al., 2007). The analysis was repeated for rural regions across the state where no day-of-week difference was observed. Table 1 lists daily concentrations relative to average weekday concentrations for the four urban regions studied here. OMI observes a larger weekend effect than the CARB monitoring stations in all four regions. A larger weekend effect as observed via satellite was also reported by Kaynak et al. (2009) in their comparison of SCIAMACHY observations and emissions. This bias observed from two different satellite instruments suggests that the surface monitoring sites may be in too close proximity to sources and are therefore not representative of the spatial pattern of NO_x in the domain. The 46% decrease observed by OMI in the South Coast Air Basin is an identical weekend effect as determined for Los Angeles by Beirle et al. (2003), Kaynak et al. (2009), and Kim et al. (2009) using observations from the GOME, SCIAMACHY, and OMI instruments.

		Sun	Mon	Tue	Wed	Thu	Fri	Sat	Weekday divided by Weekend
Sacramento	OMI	0.51	0.94	1.04	0.98	1.01	0.97	0.64	1.74
	CARB Surface	0.57	0.94	1.05	1.00	0.98	0.97	0.70	1.58
	CARB Inventory	-	-	-	-	-	-	-	1.54
San Francisco	OMI	0.51	0.82	1.02	1.02	1.05	0.91	0.64	1.74
	CARB Surface	0.53	0.91	1.00	0.99	1.04	0.97	0.67	1.68
	CARB Inventory	-	-	-	-	-	-	-	1.46
San Joaquin Valley	OMI	0.63	0.95	0.97	0.96	1.03	1.04	0.83	1.37
	CARB Surface	0.65	0.98	1.03	0.97	1.00	1.00	0.76	1.42
	CARB Inventory	-	-	-	-	-	-	-	1.70
South Coast	OMI	0.43	0.92	0.98	1.00	1.04	0.98	0.65	1.85
	CARB Surface	0.52	1.00	1.03	0.98	0.99	1.00	0.65	1.71
	CARB Inventory	-	-	-	-	-	-	-	1.53

Table 1. Daily concentrations relative to average weekday concentrations of NO_2 for summers 2005-2008 for OMI and the CARB inventory, and for summers 2005-2007 for the CARB surface observations.

Year-to-year trends in NO_2

Figure 2 (right) shows average weekday concentrations for summer 2008, which, in populated regions across the state, are visibly lower than weekday concentrations from 2005 (Figure 2 left). Fire counts from the Moderate Resolution Imaging Spectroradiometer (MODIS) indicate that the two hotspots in 2008 that do not appear in the 2005 figure (labeled with asterisks in Figure 2 right) are the result of large wildfires that burned in these regions in the summer of 2008. Together, Figure 2, shows how observations from OMI characterize changes in the spatial extent of each urban plume over time, a feature we cannot observe using surface observations alone. Using a metric of 50% of the peak of concentration of each plume to define the area, we find that the spatial extent of the Sacramento, San Francisco, and South Coast urban plumes contracted by more than 40%, while the San Joaquin Valley plume contracted by only 2% between 2005 and 2008. The 50% metric provides a consistent way to define the regions where NO_2 is elevated above background levels within all four air basins and over four years when NO_2 concentrations change dramatically. We assume that over the seasonal averages studied here, meteorology does not vary significantly from year to year.

Figure 5 shows seasonally averaged tropospheric NO_2 columns from OMI and concentrations from CARB ground stations for weekdays and weekends for the Sacramento, San Francisco, San Joaquin Valley, and South Coast regions of California. We exclude major holidays and define winter as December-February, spring as March-May, summer as June-August, and fall as September-November. The number of satellite measurements available for determining the average concentration for each season is dependent on the size of the region chosen for analysis and the proportion of cloud-free pixels available. At the low end there were 85 (64% of the inner-swath pixels) OMI observations averaged for a summer-weekend in the San Joaquin Valley and at the high end 1275 (74% of the inner-swath pixels) for a summer-weekday in the South Coast Air Basin. NO_2 surface concentrations and columns are at a maximum in winter with a minimum in the summer in the South Coast, San Francisco, and San Joaquin Valley air basins. This pattern is consistent with near constant emissions and seasonally varying OH. Conversely, for the Sacramento region, a fall maximum and spring minimum in NO_2 columns are observed while the surface network still shows a winter maximum and summer minimum. We suspect that the difference in the satellite-observed seasonal cycle in Sacramento as compared to the other three basins is related to coupling of chemical loss rates to planetary boundary layer dynamics. Modeling of NO_2 profiles and boundary layer dynamics is needed to test this hypothesis.

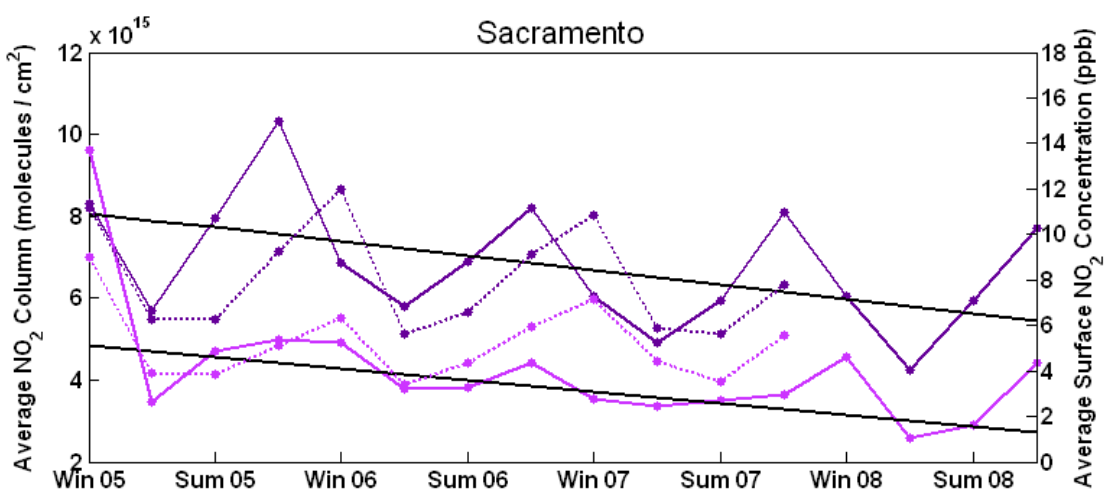

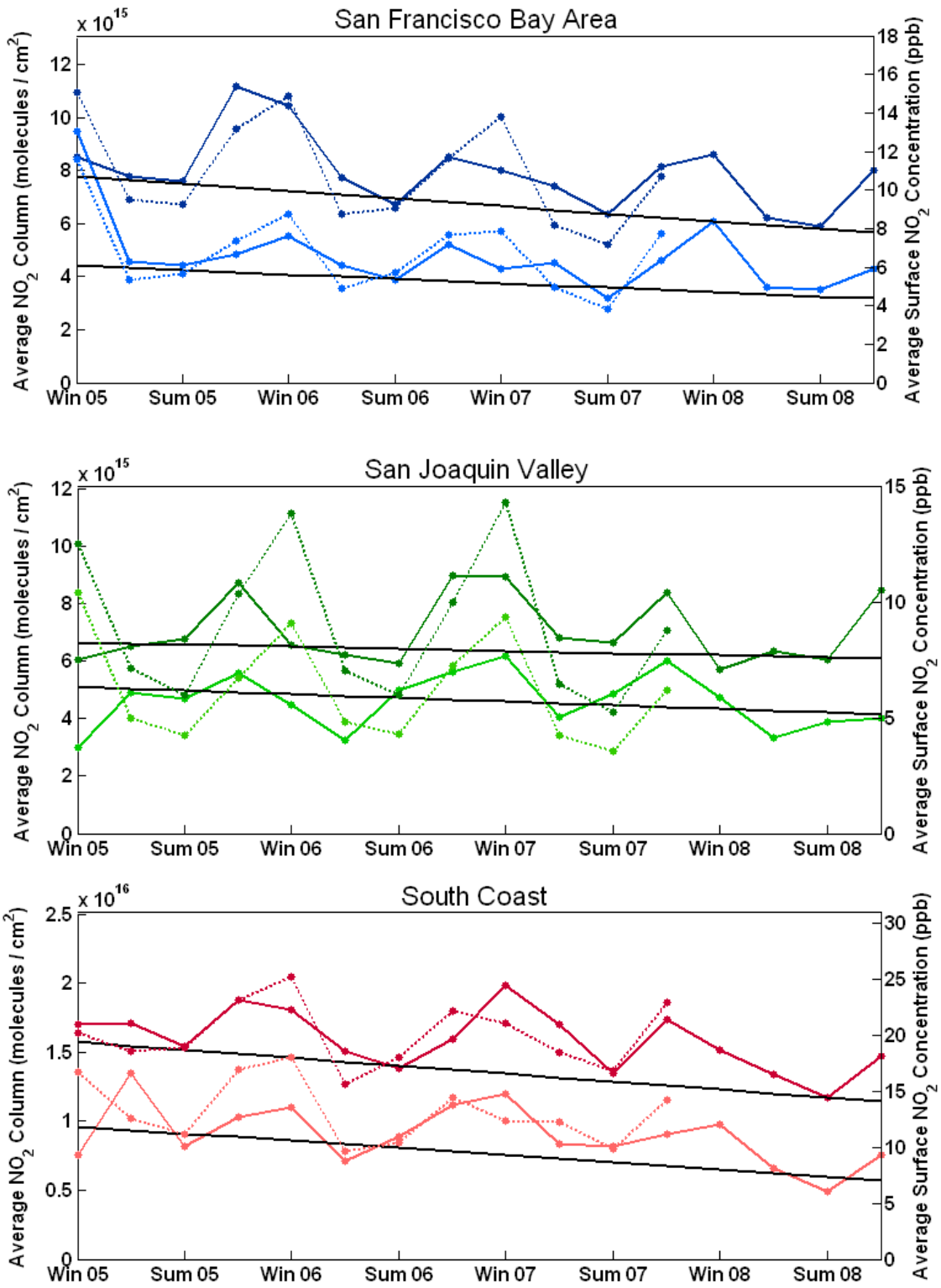

Figure 5 Average tropospheric NO_2 column concentrations (molecules cm^{-2}) from OMI (solid) and CARB (dashed) for weekdays (dark) and weekends (light) for Sacramento County, the San Francisco Bay Area, the San Joaquin Valley, and the South Coast regions of California. The trend in summers is shown by the solid black lines which have a slope of $-7.0 \times 10^{14} \pm 1.8 \times 10^{14}$ yr^{-1} and $-5.6 \times 10^{14} \pm 7.5 \times 10^{13}$ yr^{-1} for Sacramento, $-5.6 \times 10^{14} \pm 7.6 \times 10^{13}$/yr and $-3.3 \times 10^{14} \pm 1.6 \times 10^{14}$ yr^{-1} for San Francisco, $-1.5 \times 10^{14} \pm 2.1 \times 10^{14}$ yr^{-1} and $-2.5 \times 10^{14} \pm 2.0 \times 10^{14}$

yr^{-1} for San Joaquin, and $-1.1 \times 10^{15} \pm 2.0 \times 10^{14}$ yr^{-1} and $-1.1 \times 10^{15} \pm 6.3 \times 10^{14}$ yr^{-1} for South Coast for weekdays and weekends, respectively. Note that figures are on different scales to make seasonal cycles visible.

NO_x is decreasing in all regions and in all seasons as shown in Figure 6. Table 2 shows the seasonal trends in NO_2 for weekdays and weekends for each of the four regions studied and for both observational datasets and for the emissions estimates. The satellite observations indicate that there is a more consistent trend independent of season than does the surface network. Fits representing the trends for OMI summer observations are shown as black lines in the Figure 4. The trends range from –14.3% per year on weekends in Sacramento to –3.5% per year on weekdays in the San Joaquin Valley. Averaging weekdays and weekends, absolute decreases of 30.0%, 22.6%, 9.3%, and 25.9% are observed from 2005 to 2008 in the Sacramento, San Francisco, San Joaquin Valley, and South Coast, respectively. These trends have the same sign but are greater in magnitude than those observed by Kim et al. (2009) in all regions except the San Francisco region where excellent agreement is found between these two studies. Although four years is a relatively short period for examining long-term trends, clear changes in spatial pattern of NO_2 coupled with these rates of decrease observed by OMI give confidence that substantial reductions in NO_x emissions are occurring.

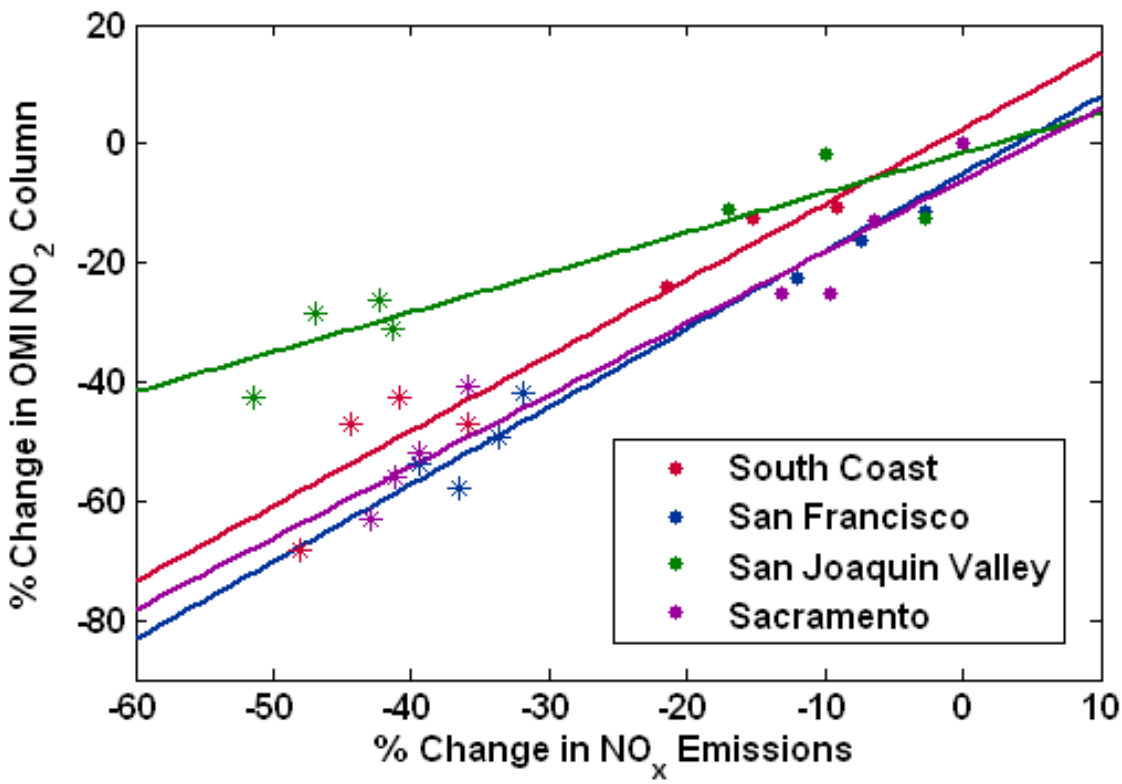

Figure 6. Percent change in emissions from CARB inventory versus percent change in OMI tropospheric NO_2 relative to weekdays in 2005 for the Sacramento, San Francisco, San Joaquin Valley, and South Coast regions. Dots show weekdays and stars weekends for 2005-2008.

Estimates of Uncertainty in OMI Observations

Agreement between satellite and ground-based observations is one line of evidence supporting the qualitative measures of NO_2 reduction derived from OMI. Observations from the surface and from space are not exactly the same, however, the extent to which the differences are due to incomplete sampling of the surface network is unknown and difficult to quantify. We propose that the complete spatial representation of urban plumes provided by satellite observation

eliminates a significant source of bias in the interpretation of trends observed by the surface network.

The robustness of each of the trends reported is also difficult to quantify directly, however, here we present several methods for indirect estimations. The smallest trends are for the San Joaquin Valley where we observe a weekday-weekend difference of 2×10^{15} molecules cm^{-2} and a decrease over four years of 5×10^{14} molecules cm^{-2}. The experimental precision of an individual OMI measurement is about 1×10^{15} molecules cm^{-2} (Boersma et al., 2009;Martin et al., 2006). The effect of this source of uncertainty is reduced by averaging over 100-1000 pixels for each value reported such that the random uncertainty is negligible compared to the variation we report.

Based on this analysis of instrument performance, we identify the dominant source of precision uncertainty in our reported values as due to meteorological variability. We know of no method for characterizing this source of uncertainty a priori. To estimate the uncertainty due to meteorological variability we note that even in the San Joaquin Valley, the seasonal cycle is recognizable and has an approximate amplitude of 2×10^{15} molecules cm^{-2}. In order to observe the seasonal cycle with the eye, we estimate that the random noise must be less than one-third the amplitude of the cycle. An alternative estimate would be to assume that trends for each season as shown in Table 1 are independent measures of the same quantity. Excluding the winter outlier, this gives a variance of approximately +/-20% yr^{-1}. A third method is to use the uncertainty in the slopes of the linear regressions for the trends reported in Table 1 and Figure 4, which indicate that the decreasing inter-annual trends we observed in all regions is robust. Finally, we can look at year to year variation in ratios. For example, we show in Figure 3 the variance in the column NO_2 for each day of the week in a given summer, normalized to the average weekday signal of that summer. The variance is approximately 15%. Taken together, these metrics indicate an overall uncertainty in basin-wide temporal trends in NO_2 columns of less than 15-20%.

Space-based constraints on Emission Inventories

CARB's emissions inventory includes seasonal and yearly changes but includes no day-of-week dependence. To compare to observations, we make the following assumptions concerning weekly emission patterns: 1) stationary, natural and area-wide sources have no day of week dependence, 2) off-road source activity are estimated using information from the NONROAD model (Janssen and Carey, 1999) and 3) on-road mobile source emissions for all four basins can be divided throughout the week using weekday/weekend traffic distribution information for the South Coast air basin (Chinkin et al., 2003). The first two assumptions are the same as those used in current emission inventories. According to Chinkin et al., the proportion of on-road total weekly activity for passenger vehicles is 15% on weekdays and 12.5% on weekends. For heavy duty trucks, the proportions are 18% on weekdays and 5.5% on weekends. Dreher and Harley (1998) found roughly the same weekday/weekend activity ratios in the San Francisco Bay Area.

The inventory (details in Figure 7) indicates that a majority of emissions in all four regions are from mobile sources. Non-mobile sources (stationary, area-wide and natural) make the largest contribution in the San Joaquin Valley where they approach 30% of the NO_x emissions on the weekends. This dominance of mobile source emissions is consistent with satellite observations which show large differences between weekdays and weekends, indicating a significant presence of anthropogenic activity that operates on a weekly cycle. Weekend emissions in this estimate are, on average, 64% of weekday emissions in 2005 in all four regions.

Between 2005 and 2008, CARB estimates that there has been no significant change in emissions from stationary, area-wide, or natural sources in California, but that mobile source emissions

have been decreasing. In the inventory, fractional decreases in gasoline and diesel NO_x emissions are similar in the Sacramento, San Joaquin Valley, and South Coast regions, roughly 7% per year. In San Francisco, gasoline is decreasing at the same 7% per year while diesel is dropping at 4% per year. Ban-Weiss et al. (2008) report changes in emissions factors of NO_x in the South Coast and San Francisco Bay areas showing that emissions factors for light duty vehicles have decreased by roughly 8% per year and those for heavy duty diesel vehicles have decreased by 3% per year. EMFAC model estimates of fuel sales from 2005 to 2008 show that sales of gasoline and diesel have not changed significantly over the time period.

		Winter		Spring		Summer		Fall	
		WD	WE	WD	WE	WD	WE	WD	WE
Sacramento	OMI	-10.7	-26.6	-9.7	-8.9	-11.8	-14.3	-8.9	-5.5
	CARB Surface	-1.3	-11.6	-3.3	6.2	-5.4	-4.0	-8.1	3.8
	CARB Inventory	-4.6	-4.3	-4.6	-4.0	-4.5	-3.7	-4.5	-4.1
San Francisco	OMI	-2.4	-16.8	-6.8	-6.3	-7.3	-7.3	-10.6	-4.6
	CARB Surface	-4.0	-18.2	-7.5	-3.5	-11.7	-16.5	-10.0	2.7
	CARB Inventory	-4.5	-4.4	-4.3	-4.1	-4.3	-3.8	-4.3	-4.1
San Joaquin Valley	OMI	1.9	16.8	0.1	-9.6	-3.5	-5.3	-1.5	-7.9
	CARB Surface	6.5	-5.3	-5.0	-7.7	-6.3	-7.8	-7.9	-3.7
	CARB Inventory	-5.6	-5.3	-5.8	-5.8	-6.1	-6.1	-5.8	-5.8
South Coast	OMI	-2.2	7.8	-5.8	-20.0	-8.1	-9.7	-6.4	-10.6
	CARB Surface	2.1	-13.2	-0.6	-1.3	-5.6	-5.8	-4.4	-8.8
	CARB Inventory	-8.1	-7.0	-7.9	-6.9	-7.6	-6.7	-7.8	-6.7

Table 2. Average percent change NO_2 per year for each season from 2005-2008.

Conclusions about CA emissions

We report spatially comprehensive satellite observations of NO_2 columns that establish trends (2005-2008) and day-of-week patterns that are strong constraints on emission patterns and photochemistry. As a further test of the connection between emissions and satellite column, Figure 6 shows the relationship between the percent change in estimated basin-wide emissions and the percent change in basin-wide tropospheric NO_2 burden observed by OMI relative to weekdays in 2005. A linear relationship between the changes in CARB estimates of emissions of NO_x and satellite column NO_2 is observed in all four regions, and weekends and weekdays fall on the same line in each basin. This implies that long-term and weekday/weekend behavior is consistent between the emissions inventory and satellite observations. The linearity when integrated over the whole domain is a useful simplification of the overall processes at work, since decreases at specific locations within the domains are not linear (as shown in Figures 1 &

2). The four domains show different relationships between emissions and column. This is due to a combination of factors including different NO_2 lifetimes associated with different OH concentrations, different planetary boundary layer heights and dynamics, and/or different wind patterns as well as the spatial patterns of emissions in each region. These factors make quantifying spatial patterns in emissions challenging, but nonetheless provide evidence that the NO_x emission inventories used in this manuscript are capturing the basin-wide trends on both daily and inter-annual timescales.

Space-based observation of the spatial distribution of NO_2 near cities reveals a larger weekend effect downwind of cities than within the city center. This effect is particularly evident near Los Angeles where we observe a large weekend effect east of Los Angeles but no weekend effect around the ports of Los Angeles and Long Beach. In the Los Angeles case, we expect that the effect can be attributed to the overwhelming influence of port emissions (which apparently vary little with day of week). This serves as an example of how the presence or absence of a day-of-week signature in a satellite observation at fine spatial resolution can be used to assess the influence of mobile versus non-mobile sources in a particular region.

Weekend reductions in NO_2 emissions inferred from the inventory are smaller than the decrease we observe from the surface and satellite measurements for all regions except the San Joaquin Valley (Table 1). Furthermore, satellite observations suggest a larger decrease over four years than estimated by the CARB inventory in Sacramento and the South Coast basin. These differences may partially be accounted for by OH feedbacks on NO_2. In a high NO_x regime, we expect OH concentrations to increase as we lower NO_x emissions, decreasing the lifetime of NO_2 and thereby further decreasing the column (Murphy et al., 2007). More work needs to be done to quantify the OH effect, however a rough estimate can be made assuming that there is a linear negative correlation between OH and NO_2 (*19*) (Murphy et al., 2007). This suggests that emission decreases are responsible for approximately 50% of the column decreases while the remainder of the decrease is due to the shorter NO_x lifetime associated with increased reaction with OH. However, it is possible that emissions are decreasing faster than the inventory suggests.

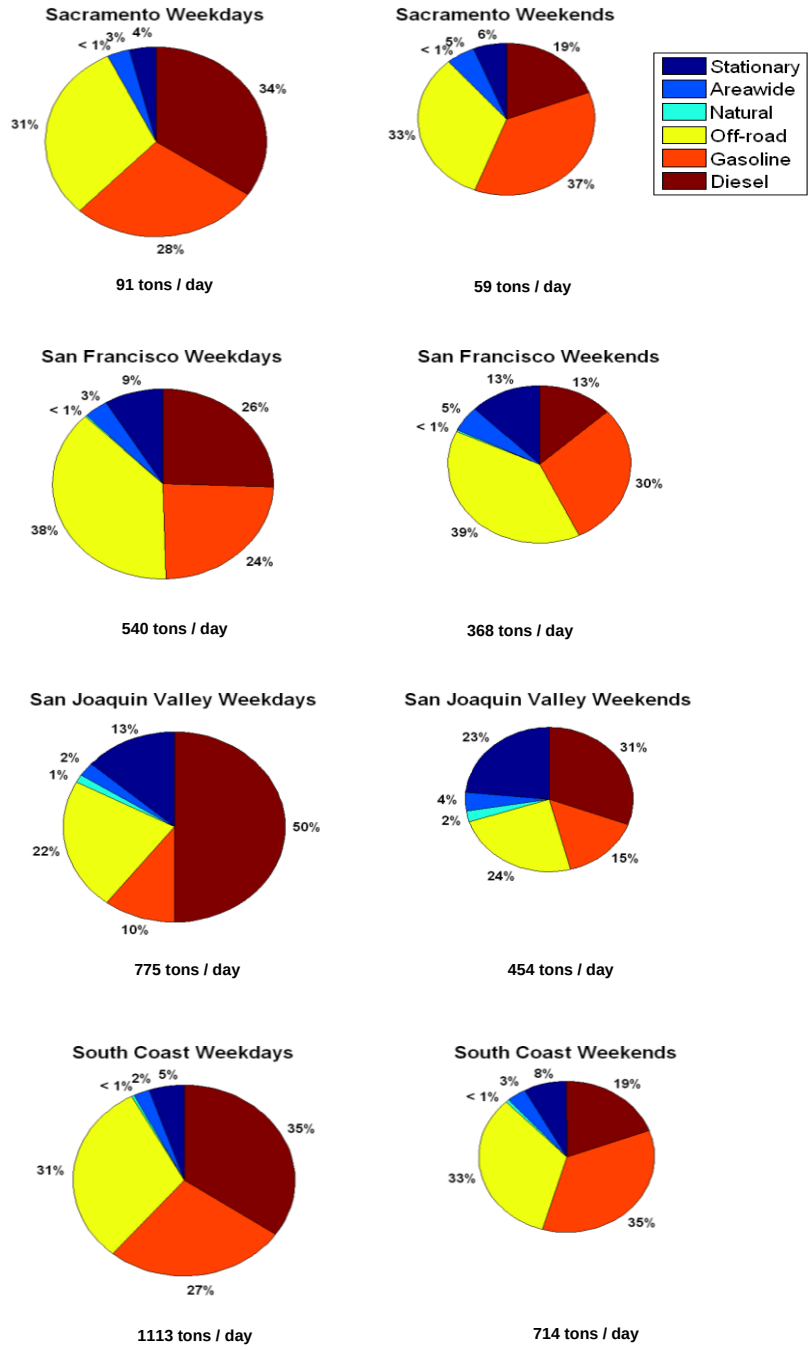

Figure 7. Distribution of emissions for weekdays in 2005 for the Sacramento, San Francisco, San Joaquin Valley, and South Coast regions according to CARB emissions estimates. Weekend charts are scaled to show how total emissions on weekends compare to weekdays.

6. Effects of spatial resolution on model/satellite comparisons

Nonlinearities in photochemical models are known to cause resolution-dependent biases in calculations of O_3. While there is an extensive body of research on the effects of model resolution on predictions of urban ozone, and a separate body of research aimed at assessing NO_x emissions from an inversion of or comparison to column NO_2 observations (Martin et al., 2003; Toenges-Schuller et al., 2006; Konovalov et al., 2006; Kim et al., 2006; Napelenok et al., 2008),

there has not to our knowledge been a systematic investigation of the combined effects of model resolution and NO_x emissions on prediction of column NO_2. Most of the inverse modeling studies conducted to date adjust NO_x emissions with the assumption that model chemistry is accurate. However, extensive research has demonstrated the strong model-resolution dependence of ozone production (P_{O3}), which has the same functional NO_x-dependence as OH (i.e., τ_{NO2}) (Kumar et al., 1994; Sillman et al., 1990; Wild and Prather, 2006). Such extensive research suggests that OH, NO_2 lifetime, and ultimately NO_2 column will vary strongly with model resolution. Consequently, emissions derived from an inverse model will have biases dependent on the resolution of the model employed. To gain an understanding of scaling relationships affecting the physics and chemistry involved, we examined the resolution required to accurately simulate NO_2 using a series of models from a simple 1-D model to WRF-CHEM.

Illustration using a 1-D plume model

To begin the discussion, we use a 1D plume model that simulates NO_2 outflow from a point source. In the 1-D model, NO_2 is emitted into the first box and transported in a constant wind field (5 m/s). We run the model for NO_2 emission rates of 0.78, 7.8, and 78 kmol hr^{-1}, at resolutions from 0.5 to 512 km in powers of 2, with dimensions perpendicular to the flow fixed at 1 km.

The photochemistry is defined using equations from Murphy et al. (2007) where NO_2 is removed by OH, which is determined by a steady-state mechanism that is a function of NO_2 concentration, P_{HOx} (1.5 x 10^7 molecules cm^{-3}), volatile organic compound (VOC) reactivity (4 s^{-1}), alkyl-nitrate branching ratio (0 %) and $[NO_2]/[NO_x]$ (0.7). Figure 8 shows OH as a function of NO_2, also indicating the corresponding NO_2 lifetime. As is well-known, at high NO_2 (red) decreasing NO_2 results in an increase of OH and a shorter NO_2 lifetime. In the intermediate-NO_2 regime (green), there is a transition from the inverse relationship of OH to NO_2 through a peak to a low-NO_2 regime (blue) where OH is linearly proportional to NO_2.

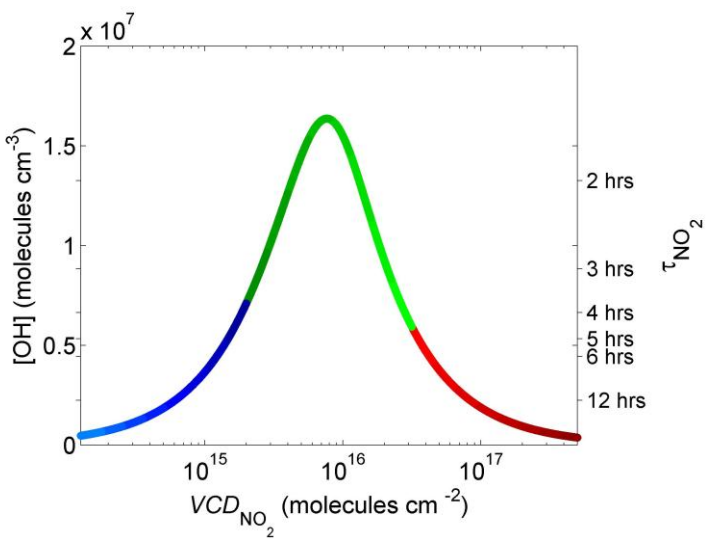

Figure 8. Steady state OH concentration (left axis) and corresponding NO_2 lifetime (1 / k_{NO2+OH} x OH, right axis) versus boundary layer column NO_2 (molecules cm^{-2}) assuming a 1-km well-mixed boundary layer.

When 1-D simulations of large (78 kmol·hr^{-1}, Figure 9a), intermediate (7.8 kmol·hr^{-1}, 9b), and small sources (0.78 kmol·hr^{-1}, 9c) are run to steady-state, NO_2 is removed by OH such that the spatial gradient reflects the applied NO_2-OH feedback following the definition previously presented (Figure 8). Failure to accurately resolve NO_2 from these sources will result in simulated OH feedback, NO_2 lifetime, and biases in NO_2 concentration that vary with model resolution and source strength.

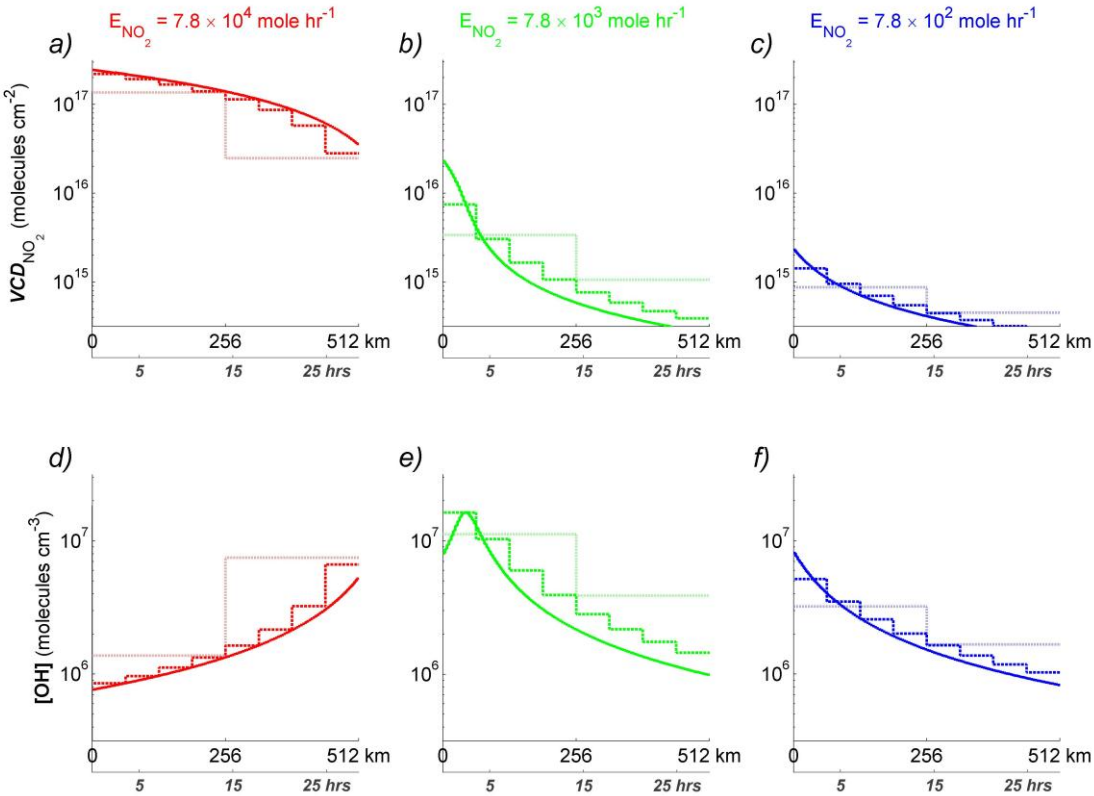

Figure 9. Predicted boundary layer VCD_{NO2} for a 1D plume model computed at model resolutions of 2 km (solid), 64 km (dashed), and 256 km (shaded) for **a)** a large (78 kmol·hr^{-1}, red), **b)** an intermediate (7.8 kmol·hr^{-1}, green), and **c)** a small (0.78 kmol·hr^{-1}, blue) NO_2 point source and **d-f)** the corresponding NO_2-OH feedback for each emission scenario as shown in Figure 8. Horizontal (N-S) and vertical layers are fixed at 1 km for all resolutions

Computed at convergent resolution (2 km), NO_2 emitted from a large source (78 kmol·hr^{-1}, Figure 9a) suppresses OH (9d) so strongly that NO_2 decays by only one e-fold in 400 km, a lifetime of 22 hours. Computed at 64 km model resolution, the concentration of NO_2 in the first grid cell is numerically diluted such that OH is larger and the NO_2 lifetime shorter and results in large biases beyond 300 km (9a). Simulated at 256 km resolution, NO_2 is numerically diluted (9a) such that OH feedback is significantly larger (9d) and NO_2 lifetime shorter (~10 hours) with domain-wide biases exceeding 50 % (Figure 10, red).

In contrast, NO_2 emitted from a small source (0.78 kmol·hr^{-1}, Figure 9c) decays rapidly when computed at 2 km resolution, a reflection of high OH feedback. At coarser model resolution (64 and 256 km), the numerical dilution results in less OH feedback (9f), a longer NO_2 lifetime, and a high-bias in NO_2 concentration (Figure 10, blue).

For an intermediate source of NO_2 computed at convergent resolution (7.8 kmol·hr^{-1}, Figure 9b), the plume decays by an e-fold within 60 km, a chemical lifetime of about three hours due to maximal OH feedback (9e). Model calculations at 64 or 256 km are not capable of resolving this sharp feature with the NO_2 concentration in the first grid cell of the 64 km simulation resulting in maximum OH feedback and the largest negative bias in domain-total NO_2 (Figure 10, green). The first grid cell of the 256 km simulation is NO_2-limited and results in a near-zero domain-averaged bias (Figure 10, green) with behavior converging towards that of the low emission scenario (blue).

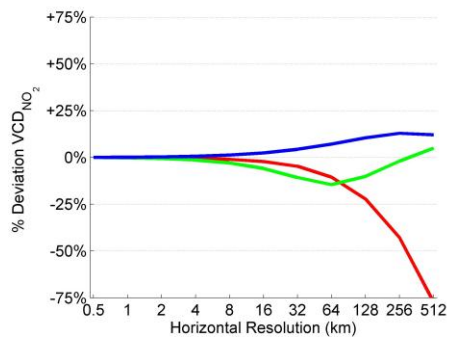

Figure 10. Resolution-dependent bias in domain-averaged NO_2 concentration versus 1D model resolution for a small (0.78 kmol·hr^{-1}, blue), moderate (7.8 kmol·hr^{-1}, green), and a large (78 kmol·hr^{-1}, red) NO_2 point source.

In a 1-D model, biases are less than 15% at model resolutions finer than 64 km and are only large (>50%) for the highest emission scenario (red) at the coarsest model resolution (Figure 10). The effects of OH on NO_2 that are evident in the 1-D model calculations are expected to affect calculations using 2 and 3-D models; we explore these next.

Illustration using a 2-D plume model

For the 2D plume model, we define a point source (2x2 km^2) in the far southwest corner (x=y=0 km) of the domain with emission rates of 1750, 175, and 17.5 kmol·hr^{-1}. NO_2 is transported with x and y wind speeds of 5 m s^{-1}, a mean flow of 5√2 m s^{-1} to the northeast, and diffused at 10 m^2 s^{-1}. The model is computed at six grid resolutions (2x2, 4x4, 12x12, 24x24, 48x48, and 96x96 km^2), with layer height fixed at 1 km. We run five model scenarios that include 1) a large source of NO_2 with OH fixed at zero to represent a conserved tracer 2) a large source of NO_2 with OH fixed at 5x10^6 molecules cm^{-3} to simulate NO_2 behavior where there is no feedback between NO_2 concentration and OH, and 3) a large, 4) intermediate, and 5) small source of NO_2 with NO_2-OH feedback applied, identical to the chemical mechanism employed in the 1D simulation (Figure 8).

In 2-dimensions, unlike 1-dimension, NO_2 is allowed to diffuse horizontally. To assess the horizontal diffusion as a function of model resolution, we simulate the advection of a conserved, non-reactive tracer, $NO_{2\text{-conserved}}$ (i.e., scenario 1, Figure 11a,c,e) and then compare to the analogous simulation with OH-feedback applied (i.e., scenario 3, Figure 11b,d,f). Particular emphasis is placed on the distribution of NO_2 with regards to OH feedback, which follows the previous definition of red, OH inversely proportional to NO_2; green, maximum-OH; and blue, OH linearly-proportional to NO_2.

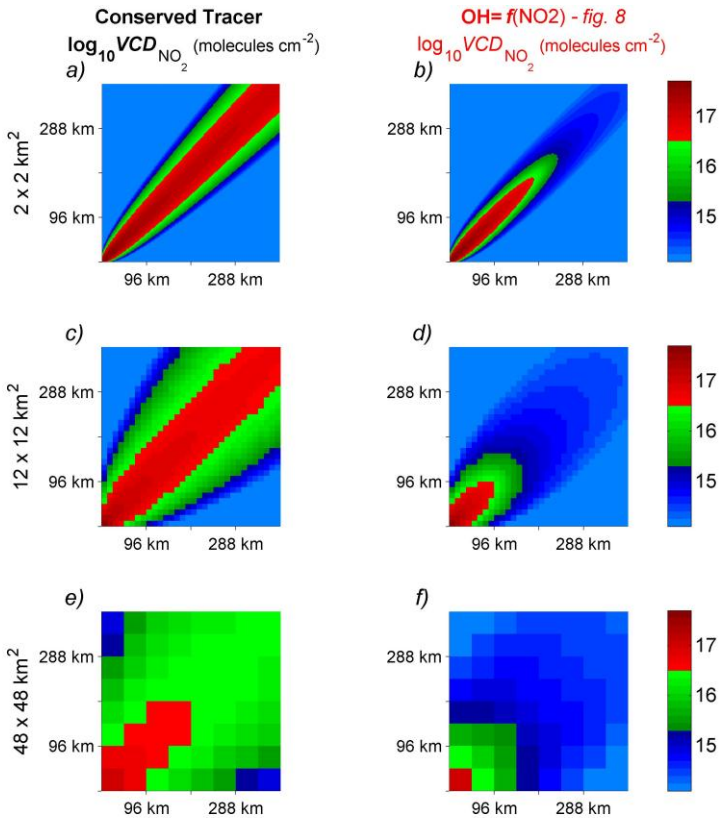

Figure 11. Column NO_2 advected from a large point source (1750 kmol·hr^{-1}), computed at 2 km resolution with **a)** OH set to 0 molecules cm^{-3} and **b)** with OH=f_{NO2} as in Figure 8. **c-d)** The same as in a-b but simulated at 12 km resolution and **e-f)** the same as in a-b but simulated at 48 km horizontal resolution. The vertical layer is fixed at 1 km for all simulations shown.

At convergent resolution (2 km), $NO_{2\text{-conserved}}$ forms a coherent, plume with a concentrated core and a steep diffusive edge (Figure 11a); Simulated at 12 km (11c), the general features of the plume are preserved, but the concentrated core is more dilute and the diffusive edge more prominent. At 48 km resolution (11e), the plume is hardly recognizable and intermediate concentrations (green) dominate the domain. Coarsening model resolution significantly affects the diffusion of $NO_{2\text{-conserved}}$.

With OH-feedback applied, NO_2 computed at 2 km (Figure 11b), much like $NO_{2\text{-conserved}}$, forms a coherent plume with a long-lived core (red) and a short-lived edge (green). At 12 km resolution (11d), the core becomes more diffuse and the short-lived edge more prominent. At 48 km resolution (11f), the plume is not recognizable, with regions of high OH-feedback (green) dominating, resulting in shorter NO_2 lifetimes and large biases.

We assess the behavior of these biases with respect to model resolution and source strength for locations including the entire domain, which is relevant to the scale of a coarse-resolution global model (Figure 12b, 384x384 km^2), 192 km nearest the source, relevant to a moderate-resolution global model (12c, x=y=0-192 km), the 96 km nearest the source, relevant to a high-resolution global model (12d, x=y=0-96 km), and a 12 km pixel downwind from the source, relevant to the scale of a satellite observation or a regional model (12e, x=y=96-108 km). We compare simulations with OH-feedback applied (red, green, blue) to one with constant OH (black, OH = 5 x 10^6 molecules cm^{-3}) to account for resolution dependent errors in transport that do not depend on non-linear NO_2-OH feedback.

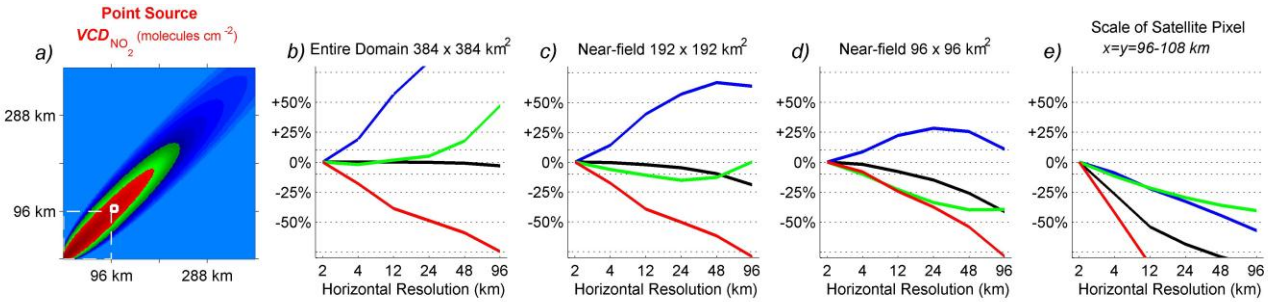

Figure 12. a) Convergent (2km) simulation of column NO_2 emitted from a large source with NO_2-OH feedbacks applied as in Figure 8. Resolution-dependent bias in NO_2 mass over the **b)** entire domain (384x384 km^2, e.g., coarse global model), **c)** the 192 km near-field (x=y=0-192 km, e.g, typical global model), **d)** the 96 km near-field (x=y=0-96 km, e.g., hi-resolution global model), and **e)** at a point downwind (x=y=96-108, e.g., a satellite observation or regional model) for NO_2 emitted from large (red), intermediate (green), and small (blue) point sources with OH = f_{NO2} as in Figure 8 and from a large point source with OH constant at $5x10^6$ molecules cm^{-3} (black).

The bias in the transport of $NO_{2\text{-constant-OH}}$ computed at 96 km is negligible over the entire domain (~0 %, 12b), significant over the 192 km nearest the source (-25%, 12c), large in the 96 km nearest the source (-45%, 12d), and dominating over a 12 x 12 km^2 pixel downwind from the source (-85 %, 12e) . When subjected to NO_2-OH chemical feedbacks (12b-e, red, green, and blue), biases diverge from that of transport alone (black) with behavior depending on the size of the emission source. For instance, at every location and spatial scale considered, simulation of a large source (red) is biased low versus transport alone (black) whereas the opposite is true for a small source (blue) with the magnitude of the bias for both increasing with coarsening resolution. These wide and varied biases result from the response of OH to the numerical dilution of NO_2 as was true in the 1-D simulations.

From this 2-D, idealized, steady-state model, we recommend that NO_2 be simulated at grid resolution no coarser than 12x12 km^2 to achieve accuracy of 25%. We now assess resolution-dependent biases of column NO_2 in fully-coupled 3D chemical transport model, WRF-CHEM.

NO_2 biases calculated with WRF-CHEM

Air quality control strategies often use 10-25% NO_x reductions as a realistic regulatory benchmark. Here, we examine the grid resolution necessary for emission inventories (12x12 km^2, 24x24 km^2, 48x48 km^2, or 96x96 km^2) for simulating column NO_2 to 10% and 25% that of a 4 x 4 km^2 inventory.

We run WRF-CHEM, a state-of-the-art multi-scale regional 3D air quality CTM (Grell et al., 2005), over the Western United States at 4 km horizontal resolution for July 1-7, 2005. To quantify the effects of NO_2-OH feedbacks on column NO_2, we vary the resolution of the gridded emissions (4, 12, 24, 48, 96, and 192 km) but maintain the resolution of model dynamics and physics (4 km) ensuring that differences in simulated NO_2 are due to chemical feedbacks. We consider only the last five days of the simulation (July 3-7). Emissions supplied for WRF-CHEM are made up by the National Emission Inventory 2005 (NEI2005) onroad and offroad transportation emissions for a typical July weekday and Continuous Emissions Monitoring (CEMS) averaged point source emissions for a typical August, 2006, weekday (ftp://aftp.fsl.noaa.gov/divisions/taq/emissions_data_2005/Weekday_emissions/readme.txt). Chemistry is driven by the mechanism developed for the Regional Acid Deposition Model, version 2 (Stockwell et al., 1990). The domain covers 2304 x 2304 km^2, of the Western US, Northern Mexico, Southern Canada and the Eastern Pacific. Biogenic emissions for all gridded emission resolutions were generated by an online module (Grell et al., 2005) at 4 km horizontal resolution for a single July day and kept constant throughout the 7-day simulation. The model

meteorology was driven by initial and boundary conditions derived from the North American Regional Reanalysis for July, 2005 (NARR – http://nomads.ncdc.noaa.gov/dods/NCEP_NARR_DAILY).

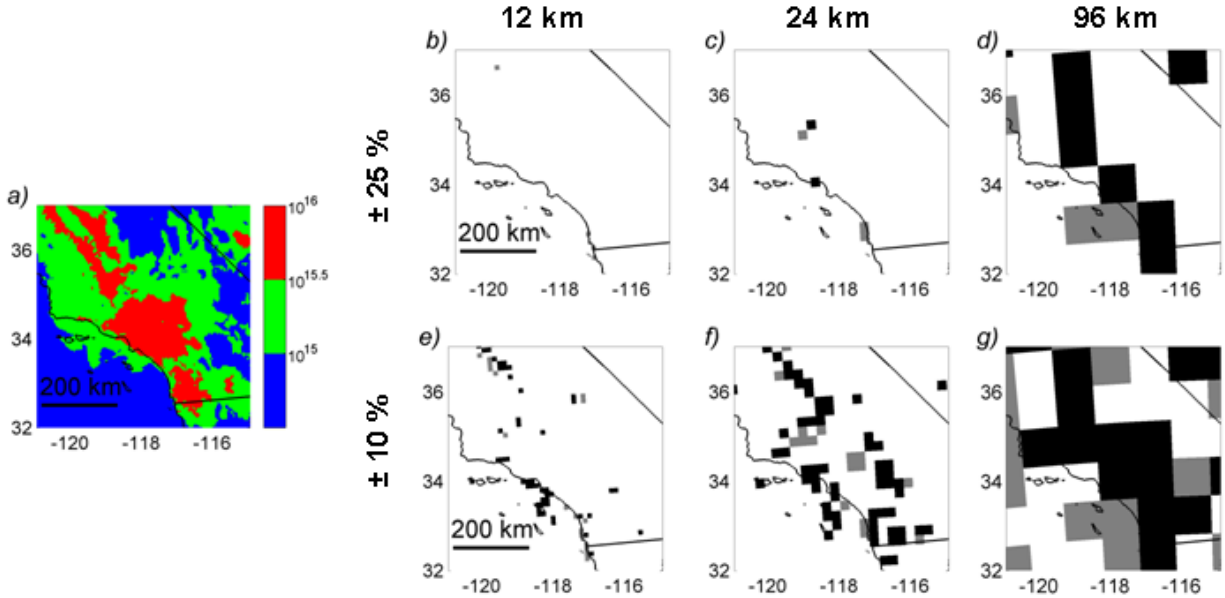

Figure 13. a) WRF-CHEM 4 km resolution simulated average 1:30 PM column NO_2 (molecules cm^{-2}) over Southern California for July 3-7, 2005. Simulated 25% biases in column NO_2 (-25%, black; +25%, gray) versus 4 km case (**a**) with model resolution set to 4 km but emissions gridded to **b)** 12, **c)** 24, and **d)** 96 km and the same for ±10% biases (**e-g**).

We assume that the resolution-dependence of chemical feedbacks is converged when emissions are gridded to 4 km and highlight where biases in predicted column NO_2 exceed 25% and 10% for emissions gridded to 12, 24, and 96 km resolution (Figures 13 and 14). These biases are most prominent where there are large gradients in the NO_2 field, particularly over the large urban centers of Southern California (Figure 13) and the coal-fired power plants in the Four Corners region in the southwest US (Figure 14). Over Southern California, a region dominated by mobile NO_x sources, prediction of column NO_2 to better than 25% (13b-d) requires that emissions are gridded to 24 km or finer while prediction to better than 10% (13e-g) requires emissions gridded to finer than 12 km near urban centers of the San Joaquin Valley and Coastal Los Angeles.

Over the coal-fired power plants of the Four Corners region in the Southwest US (Figure 14), biases exceed 25% near the sources for all gridded emission resolutions (b-d), the spatial extent of which grows with coarsening resolution. Biases greater than 10% dominate much of the plume no matter the emissions resolution (e-g); consequently accurate prediction of column NO_2 near point sources requires resolution finer than 12 km, and possibly finer than 4 km.

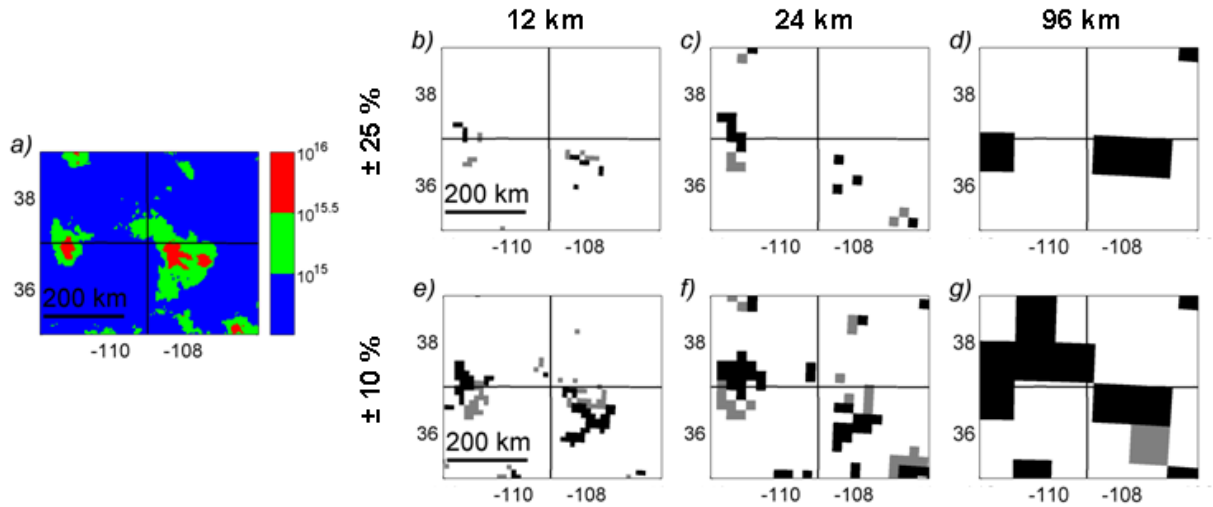

Figure 14. As in Figure 13, but for the Four Corners region of the United States.

Averaged to 96 km, biases in predicted NO_2 diverge with coarsening resolution of gridded emissions and depend on the NO_2 concentration regime (Figure 15). For regions of high NO_2 (15a-red), 30% less NO_2 is computed when emissions are gridded to 96x96 km^2 compared to that of the convergent simulation (15b, red) with individual 96x96 km^2 grid cells biased any where from 0 to 70 % lower (15b, red dots). For regions of low NO_2 (15a, blue), the average bias is less than 10 % at 96 km gridded resolution (15b, blue), but individual scenes are biased any where from -35% to +75% (15b, blue dots). For regions of intermediate NO_2 (15b, green) the bias is about -5%, while individual scenes are biased anywhere from -50% to +50% (15b, green dots).

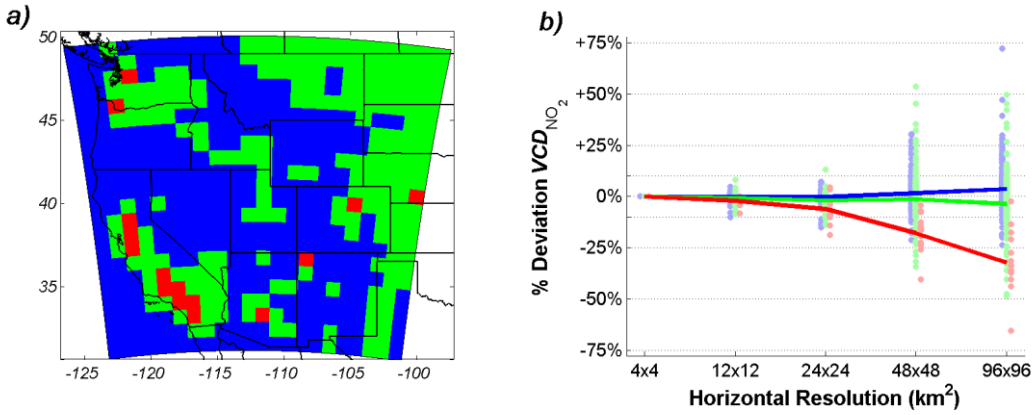

Figure 15. a) 4 x 4 km^2 WRF-CHEM column NO_2 (molecules cm^{-2}) averaged to 96 x 96 km^2 for high (red, > $10^{15.5}$), moderate (blue, $10^{15} < x < 10^{15.5}$) and low (green, < 10^{15}) NO_2 concentration regimes. **b**) Percent biases in predicted column NO_2 for the concentration regimes as determined versus horizontal resolution of gridded emissions.

These wide and varied biases (Figure 15b) indicate that NO_2-OH feedbacks are responsible for a large degree of bias in model predictions of column NO_2 and that the bias has a dependence on resolution. Emission inventories inferred from this model will suffer large biases that depend on concentration regime and model resolution due to the associated errors in chemical feedback. Accurate prediction of column NO_2 to 10% at a local scale requires emissions gridded to 4 km (13e, 14e). If comparison is made at a coarser scale (96 km), 12 km resolution is sufficient for 10% accuracy (15b). Inversion to 25% accuracy would require 12-24 km resolution at a local scale (13b-c, 14b-c) and 24 km or finer if comparison is made at 96 km scale (15b).

Summary of effects of model resolution on comparison of satellite and model NO_2 columns

We quantify the impact of NO_2-OH chemical feedbacks on NO_2 simulated by a 1D plume model, a 2D plume model, and a 3D chemical transport model, WRF-CHEM. We demonstrate that NO_2-OH chemical feedback on predicted NO_2 depends on model horizontal resolution and the magnitude of the emission source. We quantified the effect of NO_2-OH feedback on predicted column NO_2 with emissions gridded to 4, 12, 24, 48, and 96 km over the entire western US. We find that prediction of column NO_2 to 25% requires model resolution of 12 km or finer over point sources and 24 km or finer over more diffuse sources, such as a city. In this study, we find that emissions gridded to 4 km are sufficient to predict column NO_2 to 10% accuracy for all locations and sources with the possible exception of the largest point sources.

7. Emerging uses of Satellite NO_2 columns

In the course of the research pursued during this contract, we identified several other phenomena that are likely interesting constraints on models and emission inventories. We describe these below. Although our analyses are as of yet too incomplete to justify publication in the scientific literature, we expect to follow up many of these lines of inquiry with funding from other sources over the next few years and to complete manuscripts that build on these initial findings.

Spatial patterns in the "weekend" effect and model chemistry

Day of week patterns in space-based observations of column NO_2 have been used to assess the magnitude of emission sources over entire air basins with satellites (Beirle et al., 2003; Kim et al., 2009; Kaynak et al., 2009; Russell et al., 2010), and now, with the enhanced spatial resolution of OMI, we are capable of assessing the spatial variability of these day-of-week patterns within a single air basin. OMI observes that column NO_2 does not change uniformly across the Los Angles basin from weekdays to weekends (Figure 16, bottom-left); large decreases are observed along the northern and eastern edges of the basin far downwind from the largest sources while there is little observed change directly over the largest sources. One explanation for such heterogeneity is that the emissions sources themselves have a spatially heterogeneous day-of-week pattern. Another possible explanation is that decreased emissions of NO_x on weekends result in a nonlinear chemical response and a spatially heterogeneous response of column NO_2 (Figure 8). To test whether uniform decreases of NO_x emissions can lead to spatially non-uniform feedbacks in column NO_2, we run WRF-CHEM over the Los Angeles Basin for "weekday" (100% x NEI 2005) and "weekend" (62.5% x NEI2005) NO_x emissions.

Over Los Angeles, a uniform 37.5 % decrease of NO_x emissions (100 : 62.5 %) in WRF-CHEM results in a 50-60% decrease of column NO_2 downwind from the heart of the source that depends on the rate of VOC emissions (Figure 16, center and right). We are able to show that the agreement between the predicted and observed feedback patterns can be improved by modifying model chemistry. For instance, when VOC emissions are increased by a factor of two, the feedback patterns predicted by WRF-CHEM are more similar to those observed by OMI (Figure 16, bottom row). This is not to say that VOC emissions are inaccurate by a factor of two; we only use this as an example of how chemical feedbacks can affect the ratio of weekday to weekend column NO_2. Satellite-based observations of the weekend effect feedback patterns thus provide strong constraints on model chemistry.

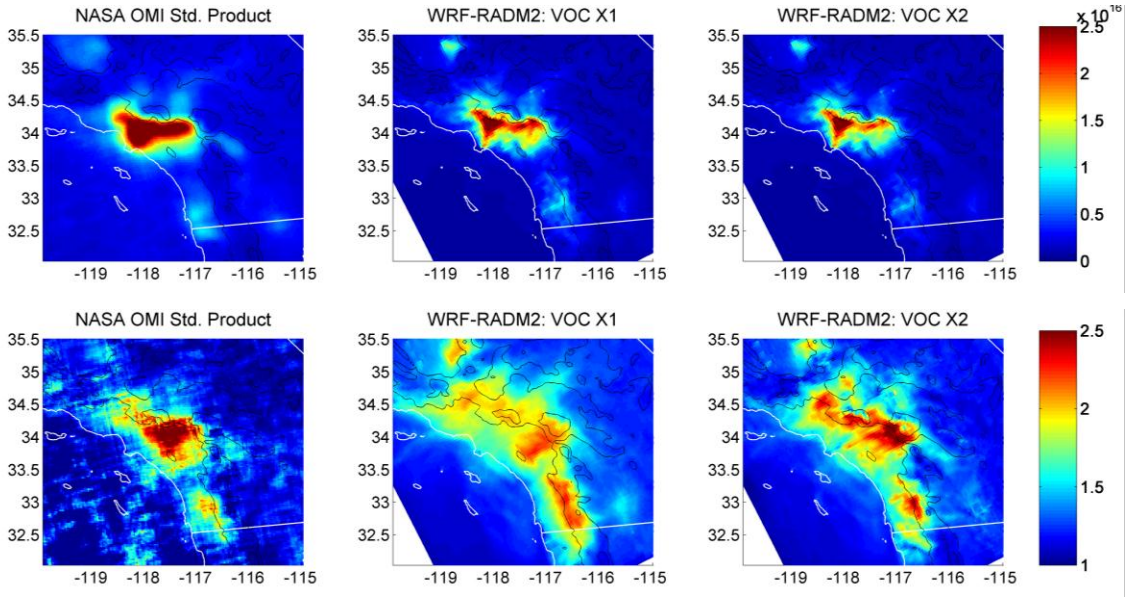

Figure 16. Top row: OMI Standard Product MJJ 2005-2008 average VCD_{NO2} (molecules cm^{-2}), WRF-CHEM VCD_{NO2} with E_{NOx} = 80% and E_{VOC} = 100% of NEI 2005, and WRF-CHEM VCD_{NO2} with E_{NOx} = 80% and E_{VOC} = 200% of NEI 2005 for a simulation run over June 10-24, 2006. Bottom row: ratio of weekday (i.e. E_{NOx} = 80% NEI for WRF-CHEM simulations) to weekend (i.e. E_{NOx} = 50% NEI for WRF-CHEM simulations) VCD_{NO2} of OMI standard product, WRF-CHEM with E_{VOC} = 100% of NEI2005, and WRF-CHEM with E_{VOC} = 200% of NEI200.

Effects of meteorology on model/satellite NO_2 comparisons

With daily global coverage and long-term observational record, OMI provides unparalleled potential to assess the impact of meteorology on column NO_2. For the United States, the National Center for Environmental Prediction assimilates a suite of metrological observations in the North American Regional Reanalysis (NARR) at 3 hr temporal and 32 km horizontal resolution (Mesinger et al., 2006). Here, we average OMI column NO_2 observations over the Four Corners coal-fired power plant (Figure 17) and for the San Francisco Bay Area (Figure 18) for days when NARR-winds are greater or less than the median wind speed. We find that the amount of NO_2 observed is strongly correlated with NARR wind speed for both the Bay Area and Four Corners Power Plant.

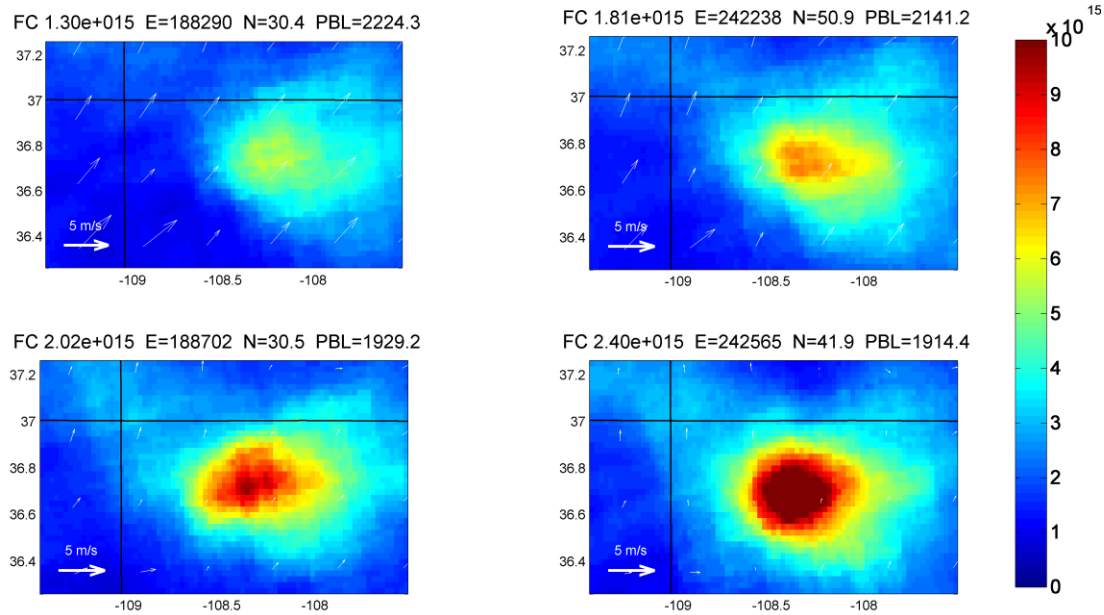

Figure 17. OMI Standard Product MJJ 2005-2008 average VCD_{NO2} (molecules cm^{-2}) of the Four Corners Power Plant region **top)** for days with wind speeds greater than the median and **bottom)** less than the median wind speed, and CEMS-observed NO_x emissions **left**) 40-75 % and **right)** 75-100% of the observed maximum. The title of each figure includes the domain-average (molecules cm^{-2}) minus a 1 x 10^{15} background, the mass of NO_x emitted (lbs) between 12AM and 1PM LST, the number of nadir observations, and the average NARR planetary boundary layer height (m). White arrows represent the NARR average wind field for days included in each average.

We use the Four Corners power plant as a test-bed for our NARR-based filtering method because it is a large source of NO_x, is required by law to report hourly NO_x emissions, and has simple chemistry compared to an urban plume. OMI-observed column NO_2 on days of low NO_x emissions (E_{NOx} = 7.2 tons hr^{-1}, Figure 17, left) is clearly lower than that of high-emission days (E_{NOx} = 9.3 tons hr^{-1}, Figure 17, right), demonstrating that OMI is accurately capturing changes in emissions. Depending on whether OMI observations are averaged over high- (Figure 17, top) or low- (Figure 17, bottom) wind days, the observed NO_2 column is very different. In fact, the column responds much more dramatically to the NARR-assimilated wind fields (Figure 17, top v. bottom) than it does to a 30 % increase in emissions (Figure 17, left v. right).

The strong correlation of observed column NO_2 with winds could be due to the effect of different mixing regimes on NO_2-OH feedbacks. At the top of a point source in the real atmosphere, a plume is on the order of meters, a power plant on the order of hundreds of meters, and concentrations of NO_x in the plume core on order of parts per thousand. Such high concentrations of NO_x will not only lead to complete titration of OH (Figure 8), but also the complete titration of ozone. Only when the plume is mixed sufficiently with the background atmosphere is steady-state O_3-NO_x chemistry reached. Even further mixing is required before NO_x reaches sufficiently low concentrations that OH is not fully titrated. In other words, the rate at which a NO_x rich power plant plume mixes with background air may determine how fast the NO_x within that plume experiences large OH feedbacks, resulting in longer NO_2 lifetimes at slower mixing rates. In that sense, the 32-km NARR wind speed product is acting as a proxy for the rates of smaller-scale mixing phenomena.

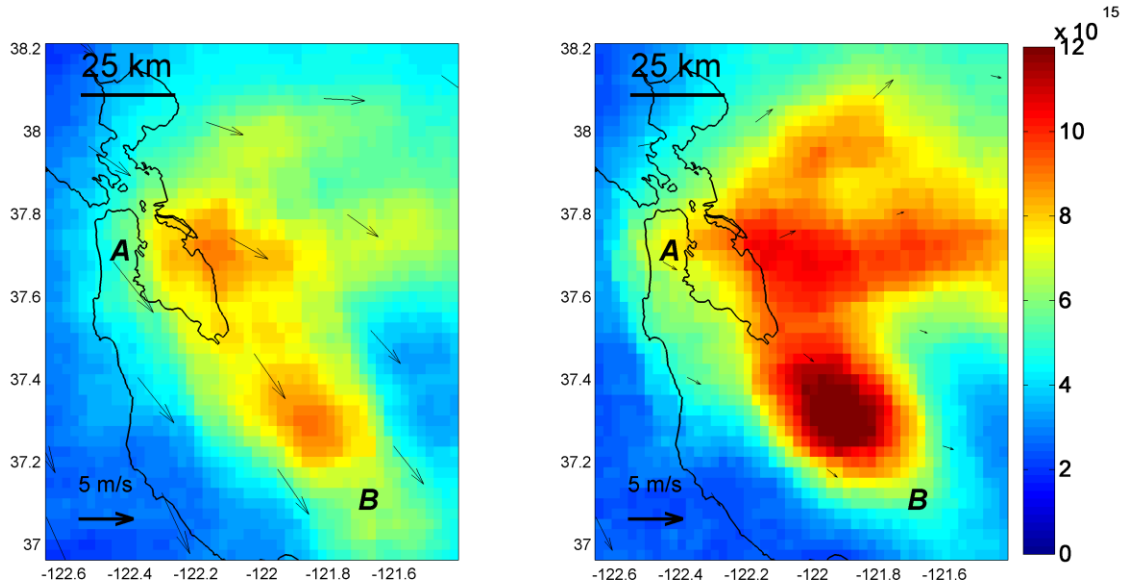

Figure 18. OMI Standard Product MJJ 2005-2008 average VCD_{NO2} (molecules cm^{-2}) of the San Francisco Bay Area **left)** for days with wind speeds greater than the median and **right)** less than the median wind speed. Black arrows represent the NARR average wind field for days included in each average.

The 2005-2008 summer average of column NO_2 observed by OMI over the Bay Area is also strongly associated with NARR-assimilated wind speeds (Figure 18). Not only does the spatial distribution of observed NO_2 change with wind speed but the total mass also decreases dramatically, as it did in the case of the power plant. Spatially, on low wind speed days, OMI observes a much stronger NO_2 signal directly over the San Francisco Peninsula (Figure 18, left, label A) that is not observed on the higher wind speed days (Figure 18, right, label A). On high wind days, the gradient in the NO_2 signal to the southeast of San Jose (left, label B) reflects the strong NW to SE flowing wind field and that of the low wind-speed days (right, label B) reflects the stagnant conditions. The differences in the observed spatial distribution of NO_2 are notable and should enable better constraints on urban-scale emissions and model transport.

While a quantitative description of these differences is not immediately available, it is likely due to the role of enhanced mixing on NO_2-OH feedbacks and the lifetime of NO_2. Unlike the power plant example (Figure 17), a city is a large source of reactive VOCs, so the impact of mixing on NO_x-VOC chemistry must be considered. To test the role of wind speed and mixing on VOC-NO_x chemistry, in the future we plan calculations using WRF-CHEM driven by assimilated NARR fields.

Variation of column NO_2 from 1 to 1:30 PM

Due to its fine spatial resolution, wide swath angle, and 16-day orbital repeat pattern, OMI offers unprecedented opportunity to observe the evolution of column NO_2 over a 30-minute time period with impressive spatial detail (Figure 19, bottom row). The 30 minute temporal coverage is achieved by binning observations made on different halves of the OMI detector, which observe a given spot on the ground with approximately 30 minutes average difference in time.

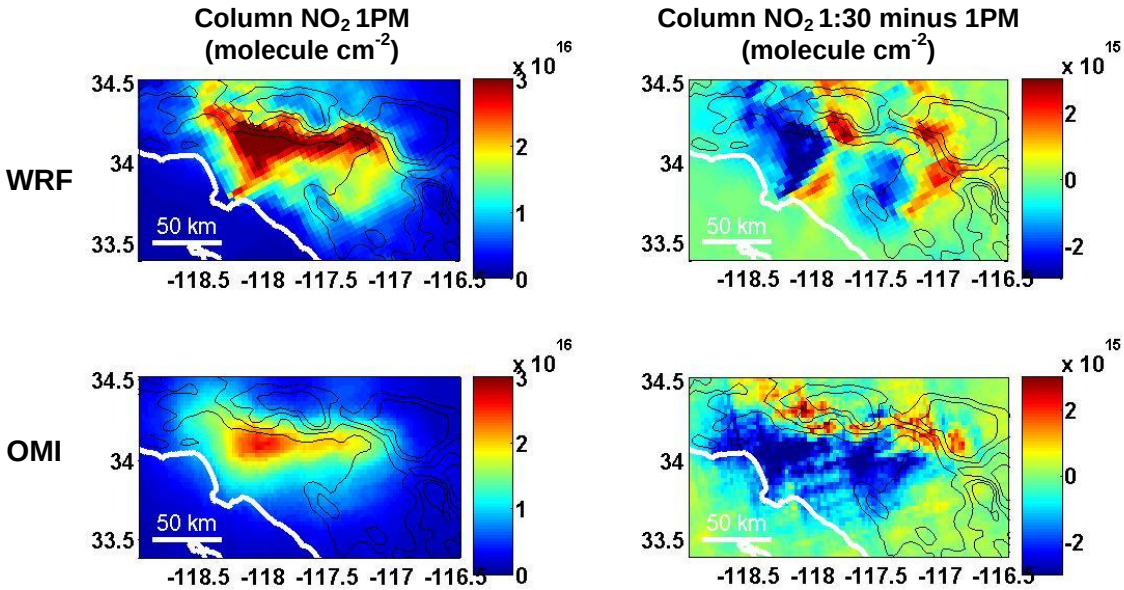

Figure 19. Column NO_2 simulated by (**top-left)** WRF-CHEM over Los Angles basin averaged at 1 pm for June 10-24, 2006 and (**bottom-left)** observed by OMI for MJJ, 2005-2008 using an in-house custom retrieval algorithm. Changes in column NO_2 from 100 to 130 PM LST using the same time periods as above simulated by WRF-CHEM (**top-right)** and observed by OMI (**bottom-right)** using an in-house custom retrieval.

OMI observed column NO_2 (Figure 19, bottom-left) is retrieved using an in-house retrieval with general treatment following that of the Standard Product (Boersma et al., 2002; Bucsela et al., 2006; Celarier et al., 2008), but with finer scale a priori databases and correction of a small error in the sign of the relative azimuth angle, an error that has only a small effect on average columns (<5%), but that biases comparison of the two halves of the detector by ~ 30%. This error has been communicated and confirmed by the NASA Standard Product team and will be corrected in future releases.

The in-house retrieval (Figure 19, bottom-left) results in much lower 1PM column NO_2 than that of the Standard Product and is therefore lower than the WRF-CHEM predictions (Figure 19, top-left), which are typically compared to the Standard Product. However, we are more interested in the spatial patterns observed than the absolute magnitude, so we can ignore this discrepancy for the purpose of this initial investigation.

Both observations and simulations show that column NO_2 is highly dynamic from 1 to 1:30 PM. From 1:00 to 1:30 PM LST, WRF-CHEM simulation shows that NO_2 mass is mostly conserved with 10-25% of two plumes being shifted from west to east (Figure 19, top-right) while OMI observations (Figure 19, bottom-right) show NO_2 mass to be decreasing significantly over most of the Los Angeles Basin with transport carrying NO_2 from south to north. This comparison of simulation and observations can be used as a constraint on model transport and chemistry.

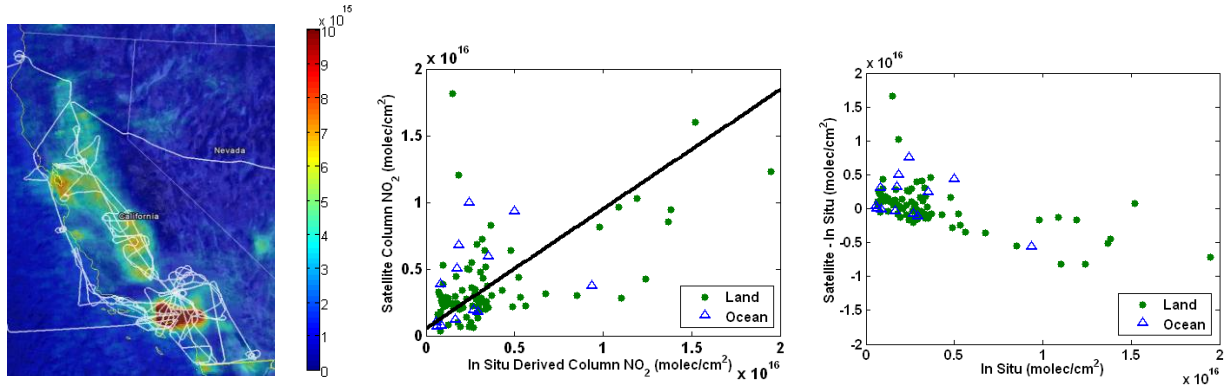

Figure 20. (a) Regional map of the OMI Standard Product tropospheric NO_2 column over California for June 2008. White lines show flight tracks flown during the ARCTAS flight campaign. (b) Aircraft derived column NO_2 versus coincident OMI Standard Product tropospheric column for the ARCTAS California flight campaign. The fit is to observations over land only, $y = 0.8939x + 5.4900\times10^{14}$, $R^2 = 0.5355$. (c) Aircraft derived column NO_2 versus the difference between the OMI Standard Product and aircraft in situ columns for ARCTAS.

Comparison of OMI columns to aircraft observations during ARCTAS-CARB

The primary means of evaluation of current retrieval algorithms have been comparison to aircraft profiles (Boersma et al., 2008; Bucsela et al., 2008; Hains et al., 2010), model predictions (Lamsal et al., 2010; Ordonez et al., 2006; Lamsal et al., 2008), and surface networks (Ordonez et al., 2006; Lamsal et al., 2008). These data sets provide limited spatial extent, preventing a full evaluation of the retrieval algorithm because coverage by surface networks is sparse as are the full vertical profiles used in previous aircraft validation.

To expand analyses using data from previous flight campaigns, we present a new approach that utilizes all aircraft observations collected in the planetary boundary layer as opposed to requiring complete profiles for comparison with satellite observations. We find that a single point in the BL is characteristic of the profile because air within the BL is generally well-mixed and contribution from the upper troposphere is small—particularly over polluted regions—as evidenced by previous aircraft measurements. Utilizing all measurements allows us to greatly expand the statistics in the evaluation of the satellite retrieval algorithm.

We estimate NO_2 vertical column densities from boundary layer aircraft observations obtained during ARCTAS for comparison with satellite-observed NO_2 columns by first co-locating aircraft measurements with coincident satellite observations. We include aircraft observations collected between 12:00pm and 3:00pm local time to coincide with the 1:45 pm OMI overpass time. We require that at least 20 seconds of aircraft measurements were collected within the boundary layer and within the spatial extent of an OMI pixel. OMI pixels flagged during the retrieval process are excluded as well as pixels with a cloud fraction greater than 20%. The boundary layer (BL) height for each aircraft observation is user-defined by identifying large changes in aircraft measured NO_2 concentration with altitude over time to determine BL entrance and exit points. We assume that the BL height varies linearly between each entrance and exit. We further assume small horizontal variability of NO_2 in the free troposphere and that the boundary layer is well-mixed. The validity of this assumption is verified using observations spanning the troposphere. Aircraft measurements taken within a single satellite pixel are averaged and integrated to determine an inferred NO_2 vertical column density.

Figure 20b shows aircraft derived tropospheric column NO_2 versus OMI Standard Product tropospheric column NO_2 for the California segment of the ARCTAS campaign. Observations

over land are indicated by green dots while observations over the ocean are shown with blue triangles. Satellite observations over water are high compared to in situ derived columns; most observations over land fall within +/- 50%. A fit to observations over land is linear (y = 1.0860 x *in situ column* – 3.5459 $\times 10^{14}$, R^2 = 0.5554).

Disagreement between aircraft and satellite observations over water is likely the result of several contributing factors. First, satellite observations over water can largely be affected by enhanced reflection off the water surface (glint) which can erroneously enhance the signal observed by the satellite. This issue is addressed in OMI documentation and a glint flag is set for pixels that may be affected. Second, NO_2 concentrations over water tend to be lower than those over land and are thereby more sensitive to instrument noise and to our well-mixed boundary layer assumption.

	NASA OMI Standard Product	**Dutch OMI DOMINO Product**	**This Work**
Terrain Reflectivity	GOME derived, 1° × 1°, Monthly	GOME derived, 1° × 1°, Monthly	MODIS, 0.05° × 0.05°, 16 day
Terrain Pressure	SDP Toolkit 90 arcsec DEM map (pressure @ center of OMI footprint)	TM4 Model, 3° × 2° (pressure @ center of OMI footprint)	GLOBE 1km^2 topo. database avg'd to OMI
NO_2 Profile	GEOS-Chem 2° × 2.5°, Annually	TM4 Model, 3° × 2°, Daily	WRF-Chem 4km × 4km, Monthly

Table 3. Terrain reflectivity, pressure and NO_2 vertical profile inputs for satellite column NO_2 retrievals.

Refined retrieval

Retrieval of NO_2 vertical column density from raw reflectance data observed from space strongly depends on viewing geometry, terrain height, terrain reflectivity (albedo), and the NO_2 vertical profile. The tropospheric column also depends on subtraction of the stratospheric component of the column. Current NO_2 column retrieval algorithms produced by the NASA Goddard Space Flight Center (GSFC) and the Netherlands Royal Meteorological Institute (KNMI) utilize terrain and profile shape databases with coarse spatial and temporal resolution (Table 3). Previous work has shown that the uncertainty introduced into the retrieved column is on the order of ~10-30% each for current terrain and profile inputs (Boersma et al., 2004; Zhou et al., 2009; Hains et al., 2010).

We have developed several new elements that are being tested and implemented into a revised retrieval for observations over CA. We have chosen to use the GLOBE (Global Land One-kilometer Base Elevation) 1km^2 topographical database, MODIS (Moderate Resolution Imaging Spectroradiometer) 0.05° × 0.05° (5600 m), 16 day averaged terrain reflectivity, and WRF-Chem monthly-averaged, 4 × 4 km^2 simulated NO_2 profiles. The MODIS albedo provides an improved spatial and temporal resolution when compared with the monthly averaged 1° × 1° GOME product currently employed in retrievals (soon to be 0.5° × 0.5°). For this dataset, we observe an average difference of +/- 54% between the terrain reflectivity in our product versus the standard product. The more spatially refined topographical database and NO_2 profiles are also expected to be more accurate than those utilized in previous retrievals (Zhou et al., 2009). We further

average each of the higher spatially-resolved datasets over the satellite pixel instead of using the value for the center of the pixel so that the parameters are more representative of the integrated pixel area. Monthly averaged WRF Chem profiles are used to eliminate the known seasonal bias in the Standard Product that exists from using yearly GEOS-Chem profiles (Lamsal et al., 2010). This work is still ongoing; however, thus far we have observed consistent improvement in the fits between satellite and in situ observations using our newly developed retrieval algorithm (Figure 21). To take this a step further, we are currently working on an improved cloud retrieval product that uses the MODIS reflectivity to determine cloud fraction and cloud height. Current cloud products rely on the coarser terrain reflectivity and are thereby less accurate than our revised product will be.

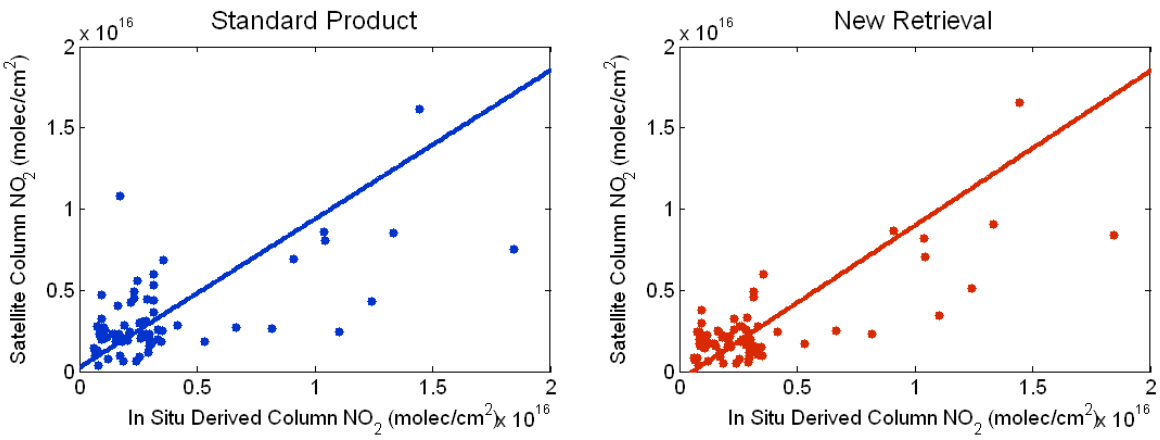

Figure 21. Aircraft derived column NO_2 versus coincident OMI tropospheric column derived over land by the Standard Product (left; $y = 0.9142x + 2.3053\times10^{14}$, $R^2 = 0.6735$) and by our revised retrieval (right; $y = 0.9514x - 5.3871\times10^{14}$, $R^2 = 0.7751$) for the ARCTAS California flight campaign.

8. Conclusions and Recommendations

In conclusion, we believe satellite NO_2 observations are an extraordinary resource for constraining emissions and chemistry affecting air quality and ozone in California. We find that satellite observations are capable of capturing long-term trends in NO_2 to allow evaluation of regulatory efforts, and of day-of-week patterns for improving model performance. For example, we find a linear relationship between changes in satellite column NO_2 and CARB emissions estimates over time, which suggests that the emissions estimates are capturing basin-wide trends on inter-annual timescales. We propose that differences between the inventory and observations in relative reduction from weekdays to weekends and inter-annual trends may be at least partially accounted for by OH feedbacks on NO_2. We quantify the impact of the NO_2-OH feedback on NO_2 using a variety of models that vary in complexity. We show that the chemical feedback is dependent on the magnitude of the emission source and on the resolution of the model. Finally, we discuss ongoing efforts to produce a new retrieval of NO_2 from OMI that utilizes more resolved spatial and temporal, terrain and profile inputs. This retrieval has shown improved correlation with aircraft observations compared with the current Standard Product.

We offer the following recommendations for future work in this area of research:

1) Models used by the CARB should be compared against remote sensing observations as part of their evaluation. We recommend that any model used for regulatory purposes capture day-of-

week and seasonal trends in addition to the magnitude of the NO_2 column. In this way, changes in emissions can be distinguished from the role of chemical feedbacks. The models should be tested against the satellite observations using monthly averages. In these averages the locations of edges will be an especially rigorous test of model performance.

2) For more quantitative analyses of the relationship between NO_x emissions and NO_2 column, models must account for the resolution-dependence of OH feedback on column NO_2. Furthermore, utilizing regional scale terrain and NO_2 profile inputs will improve the accuracy of retrieval from space-based observations.

9. References

Acarreta, J. R., De Haan, J. F., and Stammes, P.: Cloud pressure retrieval using the O_2-O_2 absorption band at 477 nm, Journal of Geophysical Research-Atmospheres, 109, 11, D05204 10.1029/2003jd003915, 2004.

Ban-Weiss, G. A., McLaughlin, J. P., Harley, R. A., Lunden, M. M., Kirchstetter, T. W., Kean, A. J., Strawa, A. W., Stevenson, E. D., and Kendall, G. R.: Long-term changes in emissions of nitrogen oxides and particulate matter from on-road gasoline and diesel vehicles, Atmospheric Environment, 42, 220-232, 10.1016/j.atmosenv.2007.09.049, 2008.

Beirle, S., Platt, U., Wenig, M., and Wagner, T.: Weekly cycle of NO_2 by GOME measurements: A signature of anthropogenic sources, Atmospheric Chemistry and Physics, 3, 2225-2232, 2003.

Board, C.E.P.A.-A.R.: The california almanac of emissions and air quality - 2009, in, edited by: Board, C.E.P.A.-A.R., Sacramento, CA, 2009.

Boersma, K. F., Bucsela, E. J., Brinksma, E. J., and Gleason, J. F.: OMI algorithm theoretical basis document, OMI trace gas algorithms, atbd-omi-04 2002, (version 2), in, 2002.

Boersma, K. F., Eskes, H. J., and Brinksma, E. J.: Error analysis for tropospheric NO_2 retrieval from space, Journal of Geophysical Research-Atmospheres, 109, D04311 10.1029/2003jd003962, 2004.

Boersma, K. F., Eskes, H. J., Veefkind, J. P., Brinksma, E. J., van der A, R. J., Sneep, M., van den Oord, G. H. J., Levelt, P. F., Stammes, P., Gleason, J. F., and Bucsela, E. J.: Near-real time retrieval of tropospheric NO_2 from OMI, Atmospheric Chemistry and Physics, 7, 2103-2118, 2007.

Boersma, K. F., Jacob, D. J., Bucsela, E. J., Perring, A. E., Dirksen, R., van der A, R. J., Yantosca, R. M., Park, R. J., Wenig, M. O., Bertram, T. H., and Cohen, R. C.: Validation of OMI tropospheric NO_2 observations during INTEX-B and application to constrain NO_x emissions over the eastern United States and Mexico, Atmospheric Environment, 42, 4480-4497, 10.1016/j.atmosenv.2008.02.004, 2008.

Boersma, K. F., Jacob, D. J., Trainic, M., Rudich, Y., DeSmedt, I., Dirksen, R., and Eskes, H. J.: Validation of urban NO_2 concentrations and their diurnal and seasonal variations observed from the sciamachy and OMI sensors using in situ surface measurements in israeli cities, Atmospheric Chemistry and Physics, 9, 3867-3879, 2009.

Bucsela, E. J., Celarier, E. A., Wenig, M. O., Gleason, J. F., Veefkind, J. P., Boersma, K. F., and Brinksma, E. J.: Algorithm for NO_2 vertical column retrieval from the ozone monitoring instrument, IEEE Transactions on Geoscience and Remote Sensing, 44, 1245-1258, 10.1109/tgrs.2005.863715, 2006.

Bucsela, E. J., Perring, A. E., Cohen, R. C., Boersma, K. F., Celarier, E. A., Gleason, J. F., Wenig, M. O., Bertram, T. H., Wooldridge, P. J., Dirksen, R., and Veefkind, J. P.: Comparison of tropospheric NO_2 from in situ aircraft measurements with near-real-time and standard product data from omi, Journal of Geophysical Research-Atmospheres, 113, D16s31 10.1029/2007jd008838, 2008.

Celarier, E. A., Brinksma, E. J., Gleason, J. F., Veefkind, J. P., Cede, A., Herman, J. R., Ionov, D., Goutail, F., Pommereau, J. P., Lambert, J. C., van Roozendael, M., Pinardi, G., Wittrock, F., Schonhardt, A., Richter, A., Ibrahim, O. W., Wagner, T., Bojkov, B., Mount, G., Spinei, E., Chen, C. M., Pongetti, T. J., Sander, S. P., Bucsela, E. J., Wenig, M. O., Swart, D. P. J., Volten, H., Kroon, M., and Levelt, P. F.: Validation of ozone monitoring instrument nitrogen dioxide

columns, Journal of Geophysical Research-Atmospheres, 113, D15s15 10.1029/2007jd008908, 2008.

Chinkin, L. R., Coe, D. L., Funk, T. H., Hafner, H. R., Roberts, P. T., Ryan, P. A., and Lawson, D. R.: Weekday versus weekend activity patterns for ozone precursor emissions in California's south coast air basin, Journal of the Air & Waste Management Association, 53, 829-843, 2003.

Cleary, P. A., Wooldridge, P. J., and Cohen, R. C.: Laser-induced fluorescence detection of atmospheric NO_2 with a commercial diode laser and a supersonic expansion, Applied Optics, 41, 6950-6956, 2002.

Cleveland, W. S., Graedel, T. E., Kleiner, B., and Warner, J. L.: Sunday and workday variations in photochemical air-pollutants in new-jersey and new-york, Science, 186, 1037-1038, 1974.

Dobber, M., Dirksen, R., Voors, R., Mount, G. H., and Levelt, P.: Ground-based zenith sky abundances and in situ gas cross sections for ozone and nitrogen dioxide with the earth observing system aura ozone monitoring instrument, Applied Optics, 44, 2846-2856, 2005.

Dreher, D. B., and Harley, R. A.: A fuel-based inventory for heavy-duty diesel truck emissions, Journal of the Air & Waste Management Association, 48, 352-358, 1998.

Dunlea, E. J., Herndon, S. C., Nelson, D. D., Volkamer, R. M., San Martini, F., Sheehy, P. M., Zahniser, M. S., Shorter, J. H., Wormhoudt, J. C., Lamb, B. K., Allwine, E. J., Gaffney, J. S., Marley, N. A., Grutter, M., Marquez, C., Blanco, S., Cardenas, B., Retama, A., Villegas, C. R. R., Kolb, C. E., Molina, L. T., and Molina, M. J.: Evaluation of nitrogen dioxide chemiluminescence monitors in a polluted urban environment, Atmospheric Chemistry and Physics, 7, 2691-2704, 2007.

Fontijn, A., Sabadell, A. J., and Ronco, R. J.: Homogeneous chemiluminescent measurement of nitric oxide with ozone - implications for continuous selective monitoring of gaseous air pollutants, Analytical Chemistry, 42, 575-&, 1970.

Gordon, A. H.: Weekdays warmer than weekends, Nature, 367, 325-326, 1994.

Grell, G. A., Peckham, S. E., Schmitz, R., McKeen, S. A., Frost, G., Skamarock, W. C., and Eder, B.: Fully coupled "Online" Chemistry within the WRF model, Atmospheric Environment, 39, 6957-6975, 2005.

Hains, J. C., Boersma, K. F., Kroon, M., Dirksen, R. J., Cohen, R. C., Perring, A. E., Bucsela, E., Volten, H., Swart, D. P. J., Richter, A., Wittrock, F., Schoenhardt, A., Wagner, T., Ibrahim, O. W., van Roozendael, M., Pinardi, G., Gleason, J. F., Veefkind, J. P., and Levelt, P.: Testing and improving OMI DOMINO tropospheric NO_2 using observations from the DANDELIONS and INTEX-B validation campaigns, Journal of Geophysical Research-Atmospheres, 115, D05301 10.1029/2009jd012399, 2010.

Harley, R. A., Marr, L. C., Lehner, J. K., and Giddings, S. N.: Changes in motor vehicle emissions on diurnal to decadal time scales and effects on atmospheric composition, Environmental Science & Technology, 39, 5356-5362, 10.1021/es048172+, 2005.

Jacob, D. J., Crawford, J. H., Maring, H., Clarke, A. D., Dibb, J. E., Emmons, L. K., Ferrare, R. A., Hostetler, C. A., Russell, P. B., Singh, H. B., Thompson, A. M., Shaw, G. E., McCauley, E., Pederson, J. R., and Fisher, J. A.: The Arctic Research of the Composition of the Troposphere from Aircraft and Satellites (ARCTAS) mission: Design, execution, and first results, Atmospheric Chemistry and Physics, 10, 5191-5212, 10.5194/acp-10-5191-2010, 2010.

Janssen, G., and Carey, P.: Weekday and weekend day temporal allocation of activity in the nonroad model., in, Report prepared for the U.S. Environmental Protection Agency, Office of Mobile Sources by Nonroad Engine Emission Modeling Team, 1999.

Kaynak, B., Hu, Y., Martin, R. V., Sioris, C. E., and Russell, A. G.: Comparison of weekly cycle of NO_2 satellite retrievals and nox emission inventories for the continental united states, Journal of Geophysical Research-Atmospheres, 114, D05302 10.1029/2008jd010714, 2009.

Kim, S. W., Heckel, A., McKeen, S. A., Frost, G. J., Hsie, E. Y., Trainer, M. K., Richter, A., Burrows, J. P., Peckham, S. E., and Grell, G. A.: Satellite-observed us power plant nox emission reductions and their impact on air quality, Geophysical Research Letters, 33, 5, L22812 10.1029/2006gl027749, 2006.

Kim, S. W., Heckel, A., Frost, G. J., Richter, A., Gleason, J., Burrows, J. P., McKeen, S., Hsie, E. Y., Granier, C., and Trainer, M.: NO_2 columns in the western united states observed from space and simulated by a regional chemistry model and their implications for NO_x emissions, Journal of Geophysical Research-Atmospheres, 114, 29, D11301 10.1029/2008jd011343, 2009.

Koelemeijer, R. B. A., de Haan, J. F., and Stammes, P.: A database of spectral surface reflectivity in the range 335-772 nm derived from 5.5 years of gome observations, Journal of Geophysical Research-Atmospheres, 108, 4070 10.1029/2002jd002429, 2003.

Konovalov, I. B., Beekmann, M., Richter, A., and Burrows, J. P.: Inverse modelling of the spatial distribution of NO_2 emissions on a continental scale using satellite data, Atmospheric Chemistry and Physics, 6, 1747-1770, 2006.

Kumar, N., Odman, M. T., and Russell, A. G.: Multiscale air quality modeling: Application to southern california, Journal of Geophysical Research-Atmospheres, 99, 5385-5397, 1994.

Lamsal, L. N., Martin, R. V., van Donkelaar, A., Steinbacher, M., Celarier, E. A., Bucsela, E., Dunlea, E. J., and Pinto, J. P.: Ground-level nitrogen dioxide concentrations inferred from the satellite-borne ozone monitoring instrument, Journal of Geophysical Research-Atmospheres, 113, D1630810.1029/2007jd009235, 2008.

Lamsal, L. N., Martin, R. V., van Donkelaar, A., Celarier, E. A., Bucsela, E. J., Boersma, K. F., Dirksen, R., Luo, C., and Wang, Y.: Indirect validation of tropospheric nitrogen dioxide retrieved from the omi satellite instrument: Insight into the seasonal variation of nitrogen oxides at northern midlatitudes, Journal of Geophysical Research-Atmospheres, 115, D05302 10.1029/2009jd013351, 2010.

Levelt, P. F., Hilsenrath, E., Leppelmeier, G. W., van den Oord, G. H. J., Bhartia, P. K., Tamminen, J., de Haan, J. F., and Veefkind, J. P.: Science objectives of the ozone monitoring instrument, IEEE Transactions on Geoscience and Remote Sensing, 44, 1199-1208, 10.1109/tgrs.2006.872336, 2006.

Marr, L. C., and Harley, R. A.: Spectral analysis of weekday-weekend differences in ambient ozone, nitrogen oxide, and non-methane hydrocarbon time series in california, Atmospheric Environment, 36, 2327-2335, 2002a.

Marr, L. C., and Harley, R. A.: Modeling the effect of weekday-weekend differences in motor vehicle emissions on photochemical air pollution in central california, Environmental Science & Technology, 36, 4099-4106, 10.1021/es020629x, 2002b.

Martin, R. V., Chance, K., Jacob, D. J., Kurosu, T. P., Spurr, R. J. D., Bucsela, E., Gleason, J. F., Palmer, P. I., Bey, I., Fiore, A. M., Li, Q. B., Yantosca, R. M., and Koelemeijer, R. B. A.: An

improved retrieval of tropospheric nitrogen dioxide from GOME, Journal of Geophysical Research-Atmospheres, 107, 4437 Artn 4437, 2002.

Martin, R. V., Jacob, D. J., Chance, K., Kurosu, T. P., Palmer, P. I., and Evans, M. J.: Global inventory of nitrogen oxide emissions constrained by space-based observations of NO_2 columns, Journal of Geophysical Research-Atmospheres, 108, 4537Artn 4537, 2003.

Martin, R. V., Sioris, C. E., Chance, K., Ryerson, T. B., Bertram, T. H., Wooldridge, P. J., Cohen, R. C., Neuman, J. A., Swanson, A., and Flocke, F. M.: Evaluation of space-based constraints on global nitrogen oxide emissions with regional aircraft measurements over and downwind of eastern north america, Journal of Geophysical Research-Atmospheres, 111, D15308 Artn d15308, 2006.

Mesinger, F., DiMego, G., Kalnay, E., Mitchell, K., Shafran, P. C., Ebisuzaki, W., Jovic, D., Woollen, J., Rogers, E., Berbery, E. H., Ek, M. B., Fan, Y., Grumbine, R., Higgins, W., Li, H., Lin, Y., Manikin, G., Parrish, D., and Shi, W.: North american regional reanalysis, Bulletin of the American Meteorological Society, 87, 343-+, 10.1175/bams-87-3-343, 2006.

Murphy, J. G., Day, D. A., Cleary, P. A., Wooldridge, P. J., Millet, D. B., Goldstein, A. H., and Cohen, R. C.: The weekend effect within and downwind of sacramento - part 1: Observations of ozone, nitrogen oxides, and voc reactivity, Atmospheric Chemistry and Physics, 7, 5327-5339, 2007.

Napelenok, S. L., Pinder, R. W., Gilliland, A. B., and Martin, R. V.: A method for evaluating spatially-resolved nox emissions using kalman filter inversion, direct sensitivities, and space-based NO_2 observations, Atmospheric Chemistry and Physics, 8, 5603-5614, 2008.

Ordonez, C., Richter, A., Steinbacher, M., Zellweger, C., Nuss, H., Burrows, J. P., and Prevot, A. S. H.: Comparison of 7 years of satellite-borne and ground-based tropospheric NO_2 measurements around milan, italy, Journal of Geophysical Research-Atmospheres, 111, D05310 Artn d05310, 2006.

Russell, A. R., Valin, L. C., Bucsela, E. J., Wenig, M. O., and Cohen, R. C.: Space-based constraints on spatial and temporal patterns of NO_x emissions in California, 2005-2008, Environmental Science & Technology, 44, 3608-3615, 10.1021/es903451j, 2010.

Sandu, A., and Sander, R.: Technical note: Simulating chemical systems in fortran90 and matlab with the kinetic preprocessor kpp-2.1, Atmospheric Chemistry and Physics, 6, 187-195, 2006.

Sillman, S., Logan, J. A., and Wofsy, S. C.: A regional scale-model for ozone in the united-states with subgrid representation of urban and power-plant plumes, Journal of Geophysical Research-Atmospheres, 95, 5731-5748, 1990.

Steinbacher, M., Zellweger, C., Schwarzenbach, B., Bugmann, S., Buchmann, B., Ordonez, C., Prevot, A. S. H., and Hueglin, C.: Nitrogen oxide measurements at rural sites in switzerland: Bias of conventional measurement techniques, Journal of Geophysical Research-Atmospheres, 112, D11307 10.1029/2006jd007971, 2007.

Stockwell, W. R., Middleton, P., Chang, J. S., and Tang, X. Y.: The 2nd generation regional acid deposition model chemical mechanism for regional air-quality modeling, Journal of Geophysical Research-Atmospheres, 95, 16343-16367, 1990.

Thornton, J. A., Wooldridge, P. J., and Cohen, R. C.: Atmospheric NO_2: In situ laser-induced fluorescence detection at parts per trillion mixing ratios, Analytical Chemistry, 72, 528-539, 2000.

Toenges-Schuller, N., Stein, O., Rohrer, F., Wahner, A., Richter, A., Burrows, J. P., Beirle, S., Wagner, T., Platt, U., and Elvidge, C. D.: Global distribution pattern of anthropogenic nitrogen oxide emissions: Correlation analysis of satellite measurements and model calculations, Journal of Geophysical Research-Atmospheres, 111, D05312 Artn d05312, 2006.

Wenig, M. O., Cede, A. M., Bucsela, E. J., Celarier, E. A., Boersma, K. F., Veefkind, J. P., Brinksma, E. J., Gleason, J. F., and Herman, J. R.: Validation of omi tropospheric NO_2 column densities using direct-sun mode brewer measurements at nasa goddard space flight center, Journal of Geophysical Research-Atmospheres, 113, D16s45 10.1029/2007jd008988, 2008.

Wild, O., and Prather, M. J.: Global tropospheric ozone modeling: Quantifying errors due to grid resolution, Journal of Geophysical Research-Atmospheres, 111, D11305 10.1029/2005jd006605, 2006.

Winer, A. M., Peters, J. W., Smith, J. P., and Pitts, J. N.: Response of commercial chemiluminescent NO-NO_2 analyzers to other nitrogen-containing compounds, Environmental Science & Technology, 8, 1118-1121, 1974.

Zhou, Y., Brunner, D., Boersma, K. F., Dirksen, R., and Wang, P.: An improved tropospheric NO_2 retrieval for OMI observations in the vicinity of mountainous terrain, Atmospheric Measurement Techniques, 2, 401-416, 2009.

10. Glossary of Terms, Abbreviations, and Symbols

AMF – Air Mass Factor, the ratio between the retrieved slant column density and atmospheric vertical column density

ARCTAS - Arctic Research of the Composition of the Troposphere from Aircraft and Satellites

CARB – California Air Resources Board

CCD – Charge Coupled Device

CEMS – Continuous Emissions Monitoring System

CTM – Chemical Transport Model

DISC – Data and Information Services Center

DOAS – Differential Optical Absorption Spectroscopy

EMFAC – Emissions Factor Model

GES – Goddard Earth Sciences

GLOBE – Global Land One-kilometer Base Elevation

GOME – Global Ozone Monitoring Experiment

GSFC – Goddard Space Flight Center

HO_x – OH + HO_2

KNMI – Netherlands Royal Meteorological Institute

KPP – Kinetic Preprocessor

LST – Local Standard Time

MODIS – Moderate Resolution Imaging Spectroradiometer

NARR – North American Regional Reanalysis

NASA ESSF – National Aeronautics and Space Administration Earth and Space Science Fellowship

NEI – National Emissions Inventory

NO_x – NO + NO_2

OMI – Ozone Monitoring Instrument

P_{HOx} – HO_x production

P_{O3} – Ozone production

SCIAMACHY – Scanning Imaging Absorption Spectrometer for Atmospheric Chartography

TD-LIF – Thermal Dissociation Laser Induced Flourescence

VOC – Volatile Organic Compound

WRF-CHEM – Weather Research and Forecasting Chemistry Model